

Agile and Cooperative Aerial Manipulation of a Cable-Suspended Load

Sihao Sun^{1*}, Xuerui Wang¹, Dario Sanalidro²,
Antonio Franchi³, Marco Tognon⁴, Javier Alonso-Mora¹

¹Delft University of Technology, Delft & 2628 CD, the Netherlands.

²University of Catania, Catania & 95041, Italy.

³University of Twente, Enschede & 7500 AE, the Netherlands.

⁴Univ Rennes, CNRS, Inria, IRISA, Rennes, 35042, France

*Corresponding author. Email: sihao.sun@outlook.com

Quadrotors can carry slung loads to hard-to-reach locations at high speed. Since a single quadrotor has limited payload capacities, using a team of quadrotors to collaboratively manipulate a heavy object is a scalable and promising solution. However, existing control algorithms for multi-lifting systems only enable low-speed and low-acceleration operations due to the complex dynamic coupling between quadrotors and the load, limiting their use in time-critical missions such as search and rescue. In this work, we present a solution to significantly enhance the agility of cable-suspended multi-lifting systems. Unlike traditional cascaded solutions, we introduce a trajectory-based framework that solves the whole-body kinodynamic motion planning problem online, accounting for the dynamic coupling effects and constraints between the quadrotors and the load. The planned trajectory is provided to the quadrotors as a reference in a receding-horizon fashion and is tracked by an onboard controller that observes and compensates for the cable tension. Real-world experiments demonstrate that our framework can achieve at least eight times greater acceleration than state-of-the-art methods to follow agile trajectories. Our method can even perform complex maneuvers such as flying through narrow passages at high speed. Additionally, it exhibits high robustness against load uncertainties and does not require adding any sensors to the load, demonstrating strong practicality.

Video of the Experiments

A video of the experiments reported in this manuscript is available at https://youtu.be/Ssi0UvC_D0I

1 Introduction

Quadrotors stand out for their unparalleled agility, speed, and mobility compared to other robotic systems. This unique capability has made them highly suitable for lifting and transporting objects to hard-to-reach locations at high speed (1, 2). However, the payload capacity of a single quadrotor is limited, prompting the exploration of utilizing multiple quadrotors in collaboration to transport (position control) and even manipulate (full pose control) heavy objects, yielding a multi-lifting system (3–5). This strategy has great potential in a wide range of applications requiring heavy object manipulation, such as construction, disaster relief, and agriculture, as well as space explorations on Mars and Titan where the flying machine has very limited resources and payload capacity (6, 7). Among the various manipulation mechanisms, the cable-suspended solution stands out for its simplicity and lightweight (8–16). By connecting each quadrotor to a different location on the load through cables, a team of three quadrotors, or more, can change the full pose of the cable-suspended load by adjusting their positions, eliminating the need for additional mechanisms like robotic manipulators.

However, existing autonomous flight algorithms can only achieve full-pose control of a cable-suspended object at low speed and low acceleration, greatly limiting its performance and endurance in time-critical missions. The main challenge lies in addressing the complex dynamic coupling and kinematic constraints between the robots, cables, and the load. Early works typically resort to a quasi-static assumption to neglect the dynamic coupling effects (e.g., (8, 17–19)), and only consider the kinematic constraints to determine the position and the path of quadrotors to reach the target pose of the load. Despite being simple, failing to account for dynamic coupling leads to undesired swinging motions, and cannot guarantee a safe load distribution on each quadrotor.

To account for dynamic coupling effects, recent works employ a force-based framework that takes into account the full dynamic model of the cable-suspended multi-lifting system. Given the reference load pose, methods in this framework calculate a desired wrench (force and torque) acting on the load through an outer-loop controller, for example, inverse-dynamics control (20), nonlinear model-predictive control (NMPC) (11, 21), and geometric control (13, 15, 22). Then the commanded wrench is allocated to each cable for their desired tension and directions through the Moore–Penrose inverse of the allocation matrix which is determined by the connection points on the load (13). Some works further exploit the system redundancy in null-space of the allocation matrix, offering capabilities to attain secondary tasks such as equal force distribution (14) and

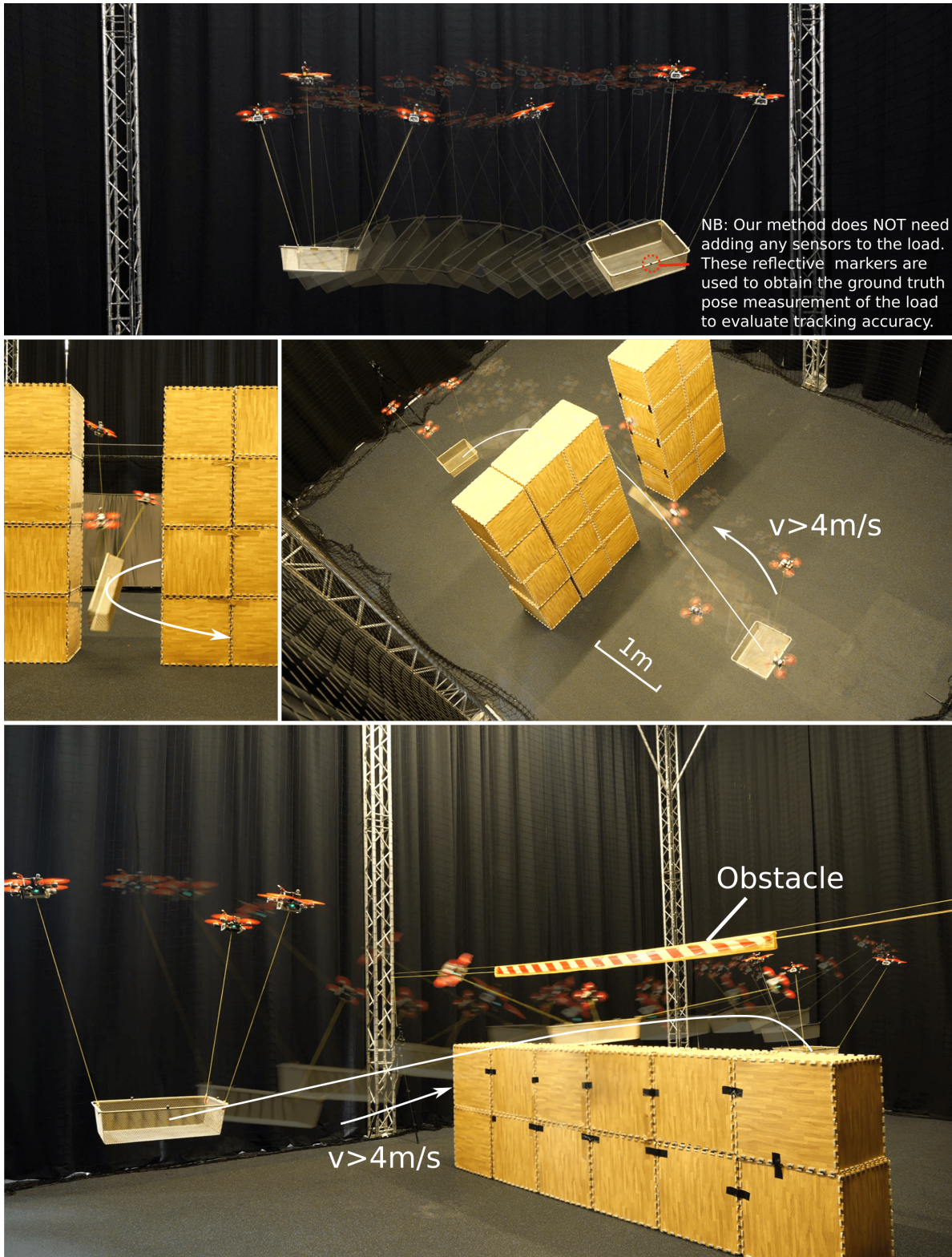


Figure 1: Snapshot of the real-world experiments. We propose an approach to control a cable-suspended using multiple quadrotors with high agility. Our approach enables full-pose control of a cable-suspended load (**top**), and allows the quadrotors to carry the load to dynamically fly through a narrow passage (**middle**) and fly through a horizontally oriented gap (**bottom**) at high speed. Please check Movie S1 for the video.

obstacle avoidance (11, 15) while retaining the collective wrench on the load. Once the required tension and cable directions are determined, a mid-level controller calculates the command thrust and attitude for each quadrotor, which are then executed by an inner-loop attitude controller. However, despite considering the dynamic-coupling effects, the force-based methods are still far from fully exploiting the cable-suspended system’s high agility. In fact, only low-speed (under 1.5 m/s) and low acceleration (under 0.5 m/s^2) flights have been successfully demonstrated in real-world experiments for full-pose control using force-based approaches (11, 15, 22). Given that a loaded quadrotor with a thrust-to-weight ratio of 1.5 can easily reach an acceleration of over 4 m/s^2 , existing solutions still largely compromise the inherent agility of quadrotors, making the cable-suspended multi-lifting system far from operating in time-critical missions.

Here, we identify three major challenges obstructing the existing methods to achieve high agility in reality. First, the aforementioned force-based methods typically employ a cascaded control structure, which assumes that the load dynamics are significantly slower than those of the quadrotor. This assumption fails during agile flights, where the load needs to change its pose rapidly. With a cascaded control structure, the outer-loop commands can easily exceed the bandwidth of the inner loops, leading to instability, particularly in the presence of communication delays and actuator dynamics, which are often overlooked in simulation studies.

The second challenge is the high reliance on an accurate dynamic model which is difficult to obtain. The mismatch of the model, especially the mass and inertia of the payload, leads to an error in the thrust command sent to each quadrotor, ultimately causing tracking error and even instability.

The third challenge is the reliance on high-frequency load and cable measurements for closed-loop control, requiring additional sensors to be installed onto the load, such as reflective markers for motion capture system (14, 15, 22); or installing additional sensors on the quadrotors, such as downward facing cameras (10), cable tension sensors and cable direction sensors (23, 24). These methods inherently suffer from sensor noise and latency and typically require non-trivial engineering efforts for installation and calibration, making them largely impractical for day-to-day real-world operations.

1.1 Trajectory-based framework

In this article, we propose a trajectory-based framework to address the above challenges. This framework separates the controller into two submodules: an online kinodynamic motion planner, and onboard trajectory tracking controllers. The kinodynamic motion planner considers the whole-body dynamics of the cable-suspended multi-lifting system, including the force-coupling effects, to generate dynamically feasible trajectories to each quadrotor in a receding horizon fashion. Then, a trajectory tracking controller is deployed onboard each quadrotor to generate the rotor-speed-level commands to follow the online generated trajectories while considering the effect of the cable forces.

Specifically, we formulate the kinodynamic motion planner into a finite-time optimal control problem (OCP) which can be effectively solved within tens of milliseconds to generate predicted trajectories with a horizon of 2 s. The OCP formulates safety-related constraints as path constraints, including thrust limitations, cable tautness, non-internal collisions, and obstacle avoidance. As the planner also takes into account the bandwidth and actuation constraints of the inner loop, the assumption of the time-scale separation principle required by existing solutions can be circumvented. The generated trajectories include the full state of quadrotors along the horizon, hence our method allows the planner to run at a significantly lower frequency ($\leq 10\text{Hz}$) than the outer-loop controllers of existing works ($\geq 100\text{Hz}$). This makes our method remarkably more robust against the delay and noise on the state estimate of the load.

We deploy an estimator based on an extended Kalman Filter (EKF) that fuses the whole-body dynamic model and the inertia-measurement-unit (IMU) data on quadrotors to provide satisfactory state estimates for the planner and achieve high-accuracy closed-loop tracking accuracy outperforming state-of-the-art methods. The onboard trajectory tracking controller employs the incremental nonlinear dynamic inversion (INDI) technique (25–27) and leverages the differential-flatness property of quadrotors (28) to follow the reference trajectories and instantly compensates for the forces from cables using IMU data. The mismatch in the planned cable tension that stems from the possible mismatch of the load inertia model is thereby effectively compensated for by the trajectory tracking controller, which eventually ensures high robustness against model uncertainties.

In the remainder of this article, we study the performance of the proposed trajectory-based framework in real-world experiments. The results reveal that the cable-suspended multi-lifting system controlled by our framework can achieve unprecedented agility in pose control and trajectory following at high speeds (over 5 m/s) and accelerations (over 8 m/s²). It can even rapidly change configurations to avoid obstacles and fly through narrow passages dynamically (Fig. 1). Moreover, the experiments were conducted without carefully measuring the load’s inertia properties or adding any sensors to the load to measure its pose, enhancing practicality in day-to-day real-world operations. The results are summarized in Movie S1.

2 Results

2.1 Experimental Setup

We test our algorithm through real-world experiments using three quadrotors to manipulate a 1.4 kg payload. Each quadrotor, weighing 0.6 kg, experiences a significant additional force due to the payload. Without loss of generality, we set the cable length to 1 m for all quadrotors. These cables are attached to three distinct points on the rigid-body payload to enable pose control, with the other end connected to each quadrotor 0.03 m below its center of gravity (CoG). The quadrotors are

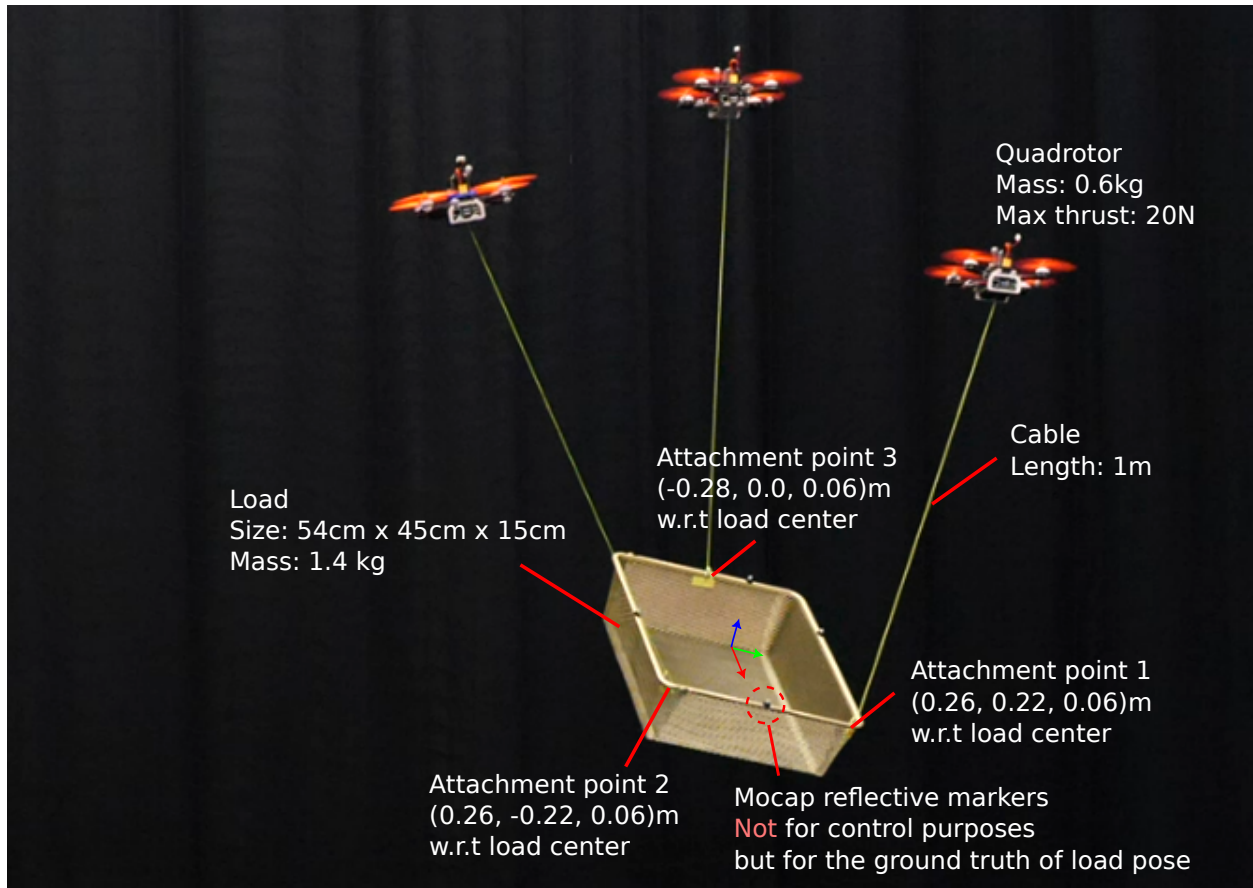


Figure 2: Experimental setup. A snapshot of our experiment, together with the parameters of the load, the quadrotors, and the cables.

Table 1: Position tracking result. Position root-mean-square-error (RMSE) in tracking references with different levels of agility. All reference trajectories are with a figure-eight shape. Our method significantly outperforms the two benchmark methods (Geometric (13), and NMPC (11)), especially in tracking agile trajectories. The benchmark methods are tested in a simulation environment while our methods are tested in both simulation and real-world experiments.

Name of <i>Ref.</i> trajectories	vel_{\max} [m/s]	acc_{\max} [m/s ²]	$jerk_{\max}$ [m/s ³]	Geometric (13) [m]	NMPC (11) [m]	Ours [m]	Ours (real-world) [m]
Slow	1	0.5	0.25	0.0375	0.0470	0.0345	0.0810
Medium	2	2	2	0.119	0.143	0.0608	0.0886
Medium+	2	4	8	Crash	Crash	0.0661	0.114
Fast	5	8	16	Crash	Crash	0.118	0.193

modified from the Agilicious open-source hardware platform (29), and each operates its onboard algorithms using a Raspberry Pi 5 mini PC. The centralized planner for our algorithm runs on a laptop at 10 Hz, sending commands to each quadrotor via WiFi.

The experiments were conducted in a controlled environment using motion capture systems for state estimation of the quadrotors only. The pose of the load for closed-loop control is estimated *without* relying on the motion capture system. Nonetheless, reflective markers are still attached to the load to log its ground-truth pose. A snapshot of the experimental setup is provided in Fig. 2.

2.2 Agile Pose Control

To demonstrate that our method can control the cable-suspended multi-lifting system to achieve high agility, we test its performance in tracking eight-shaped trajectories with various levels of agility (increasing velocities, accelerations, and jerks), listed in Table 1. At the same time, the heading also varies over time with a constant yawing rate of 0.25 rad/s. We present the result of our method in real-world experiments. We also present the result of our methods compared with two benchmark methods obtained in a simulation environment. It is worth noting that the parameters of the quadrotors and loads in these experiments are kept consistent across different approaches to ensure a fair comparison.

We select two representative state-of-the-art methods as the benchmark: geometric control (13, 22) and NMPC (11) that have been successfully demonstrated in real-world experiments. These two force-based approaches both employ a conventional cascaded structure, namely using an outer-loop controller to generate the desired collective load wrench through a geometric controller or NMPC and distribute it to each quadrotor through an inner-loop controller. Table 1 lists the tracking error in these reference trajectories. Both baseline approaches can follow trajectories with relatively low agility (up until $v_{\max} = 2$ m/s, $a_{\max} = 2$ m/s²). However, they started to fail in

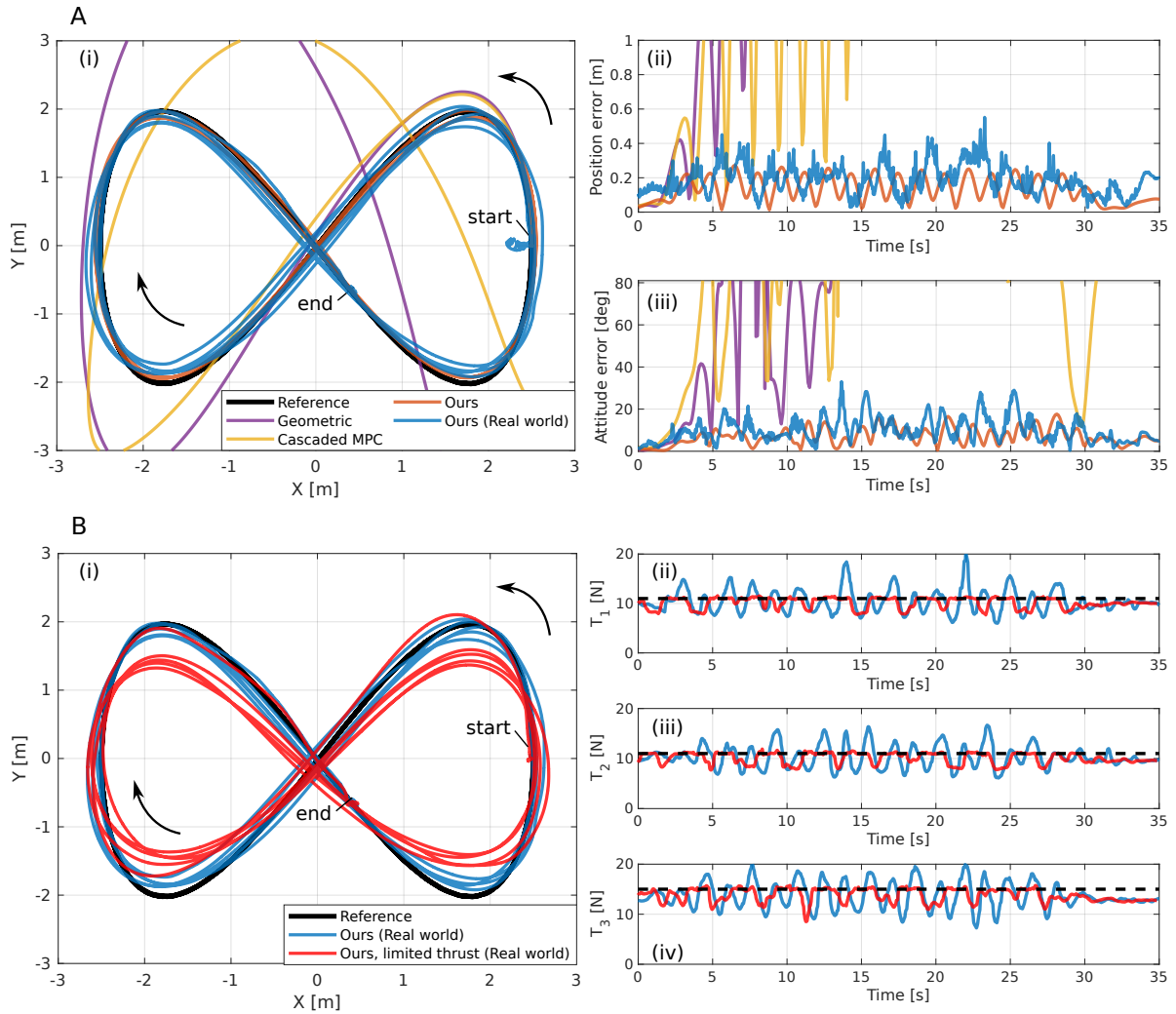


Figure 3: Performance in tracking the reference *Fast*. (A)(i) Top view of the flight path of the CoG of the load while tracking a figure-eight trajectory with a maximum speed of 5 m/s and a maximum acceleration of 8m/s^2 . Both benchmark methods failed in tracking this agile trajectory while our method succeeded in both real-world experiments and simulation.(ii-iii) Time history of the root-mean-square-error of the load position and attitude tracking error of the load. We use axis-angle representation and present the time history of the angles of the attitude error. (B) (i) Top view of the flight path in real-world experiments without and with limited thrust. Once the maximum thrust is limited, the reference trajectory becomes dynamically infeasible for the system to follow accurately (red). Our method automatically controls the load to cut corners to reduce the required acceleration while keeping up with the reference. (ii-iv) The commanded collective thrust of the three quadrotors with the reduced thrust limits (black dash lines).

following the reference trajectories *Medium+*, which involve higher peaks in acceleration and jerk, requiring rapid changes in cables’ directions to produce a fast time-varying wrench on the load. Our method, by contrast, avoids using the cascaded structure employed by the benchmark methods, and thus can consequently allow fast variation of load pose and cable directions. Therefore, it still successfully follows trajectories *Medium+* and even the reference *Fast* which has significantly larger accelerations and jerks. A video recording of the comparison in simulation environments is provided in Movie S2.

Fig. 3A presents the path and pose error while tracking *Fast* that has a maximum velocity of 5 m/s and a maximum acceleration of 8 m/s². The reference velocity and acceleration started from zero and gradually reached their maximum values. As the reference velocity increased, both baseline methods failed to track the reference. By contrast, our method succeeds in tracking the reference trajectory with a position-tracking root-mean-square-error (RMSE) of 0.193 m, and an attitude-tracking RMSE of 11.1 deg, in real-world experiments. The high closed-loop tracking accuracy results from the combined efforts of our controller and estimator. The time history of pose reference, estimate, and ground truth are presented in Fig. 4.

Our algorithm considers dynamic coupling and thrust limits to prevent overloading the quadrotors. We limit the maximum thrust of the three quadrotors from 20 N to 11 N, 11 N, and 15 N respectively, while tracking the reference *Fast*. (The third quadrotor lifts the load alone on the opposite side of the other two, requiring it to produce higher thrust). Consequently, the reference trajectory becomes dynamically infeasible for the multi-lifting system to follow precisely. The tracking result is presented in Fig. 3B. Despite these thrust limitations, our method still enables the multi-lifting system to approximate well the reference trajectory and avoid instability. Interestingly, our method lets the load “cut the corner” to follow the reference at a lower acceleration. Throughout this process, our method ensures that the commanded thrust of each quadrotor remains within the reduced thrust limits. Additionally, the variation in the collective thrust of each quadrotor is significantly reduced with a tightened thrust limit, demonstrating that our method automatically adjusts the level of agility to match the capabilities of the quadrotors.

2.3 Load Pose Estimation Results

In the above experiments (all real-world experiments shown in this paper), we need information on load pose and twist to achieve dynamic and accurate trajectory tracking. In the state-of-the-art method that includes real-world experiments, additional sensors are required for the load pose estimation. The most commonly used approach is attaching reflective markers on the load to measure its pose from the motion captures system (11, 15, 19), or resorting to additional downward-facing cameras and attaching additional circular tag on the load (10). However, it is impractical to attach these sensors in the field for day-to-day use.

In comparison, our algorithm does not need to put any additional sensors on the load, nor

does it make any modifications to the quadrotors. We demonstrate that by simply leveraging the inertia-measurement-unit (IMU) on each quadrotor and the dynamic model of the multi-lifting system can provide a sufficiently accurate load pose and twist estimate as well as the cable states to achieve agile pose control. Fig. 4 presents the comparison between the ground truth pose of the load and the estimated pose while tracking the "Fast" reference trajectory. Despite the large acceleration of the motion, over 45 degrees of inclination, and continuous yawing motion, our method can provide sufficiently high estimation accuracy to achieve closed-loop trajectory tracking. The position estimation RMSE is 0.136 m and the attitude estimation RMSE is 7.5 deg even with the highly dynamic motion of the system.

2.4 Obstacle Avoidance

Our algorithm enables high-speed obstacle avoidance without designing obstacle-free trajectories in advance, which require hundreds of seconds to generate for a multi-lifting system composed of more than three quadrotors (15). Instead, we encompass the obstacles with pre-defined no-fly zones and formulate them as second-order inequality constraints in the OCP. This way, the online-generated reference trajectories for the quadrotors ensure that both the quadrotors and the load avoid the no-fly zones, thereby preventing collisions with the obstacles.

We demonstrate the obstacle avoidance capability of our algorithm in two unprecedentedly explored challenging tasks. In both tasks, the multi-lifting systems must navigate through gaps smaller than their original configuration size. Therefore, the kinematic redundancy of the system needs to be leveraged to change the configuration in these tasks to squeeze through the narrow passage. In the second task, the traversal must be completed dynamically to leverage the momentum gained at high speed to fly through, as the system cannot counteract gravity with its configuration at the moment of traversal if it attempts to fly statically.

2.4.1 Flying through a narrow passage

In the first scenario, the multi-lifting system needs to fly through a narrow passage with a width of 0.8 m. Note that the width of the entire multi-lifting system in hovering condition is approximately 1.4 m, which is greater than the size of the gap. We first commanded the quadrotors to carry the load to hover at an initial pose. Then we set a target pose at 6 m away from the initial position along the y axis of the inertial frame. A reference trajectory of the load is generated from the initial pose to the target pose using the minimum snap algorithm (28). However, this reference trajectory intersects with the obstacle. Without an obstacle avoidance mechanism, the system will directly fly towards the wall and crash. To guide the system through the opening, we define two vertical cylinders as no-fly zones, each with a radius of 1.5 m, encompassing the real obstacles. These two no-fly zones create a gap of 0.2 m for the system to pass through, ensuring a 0.3 m clearance

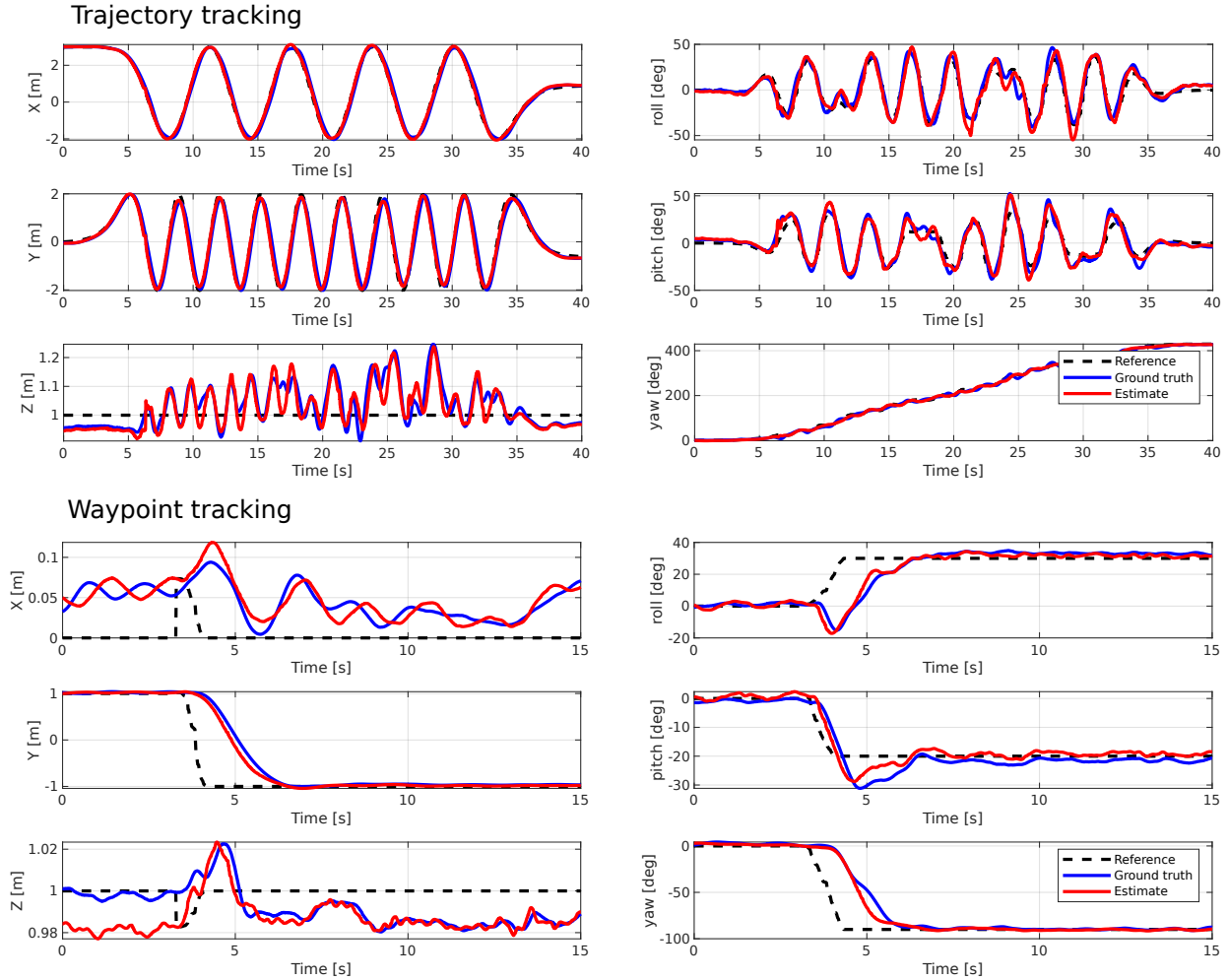


Figure 4: Load pose estimation and tracking result. Without adding additional sensors to the load or force sensors to quadrotors, our algorithm can accurately estimate the load’s pose for an accurate closed-loop control. **Top:** time history of the position and attitude (Euler angles) estimate in comparison with the ground truth from the motion capture system, as well as the reference load pose while tracking the figure-eight trajectory *Fast*; **Bottom:** time history of the estimated, the ground truth, and the reference load pose while tracking a setpoint.

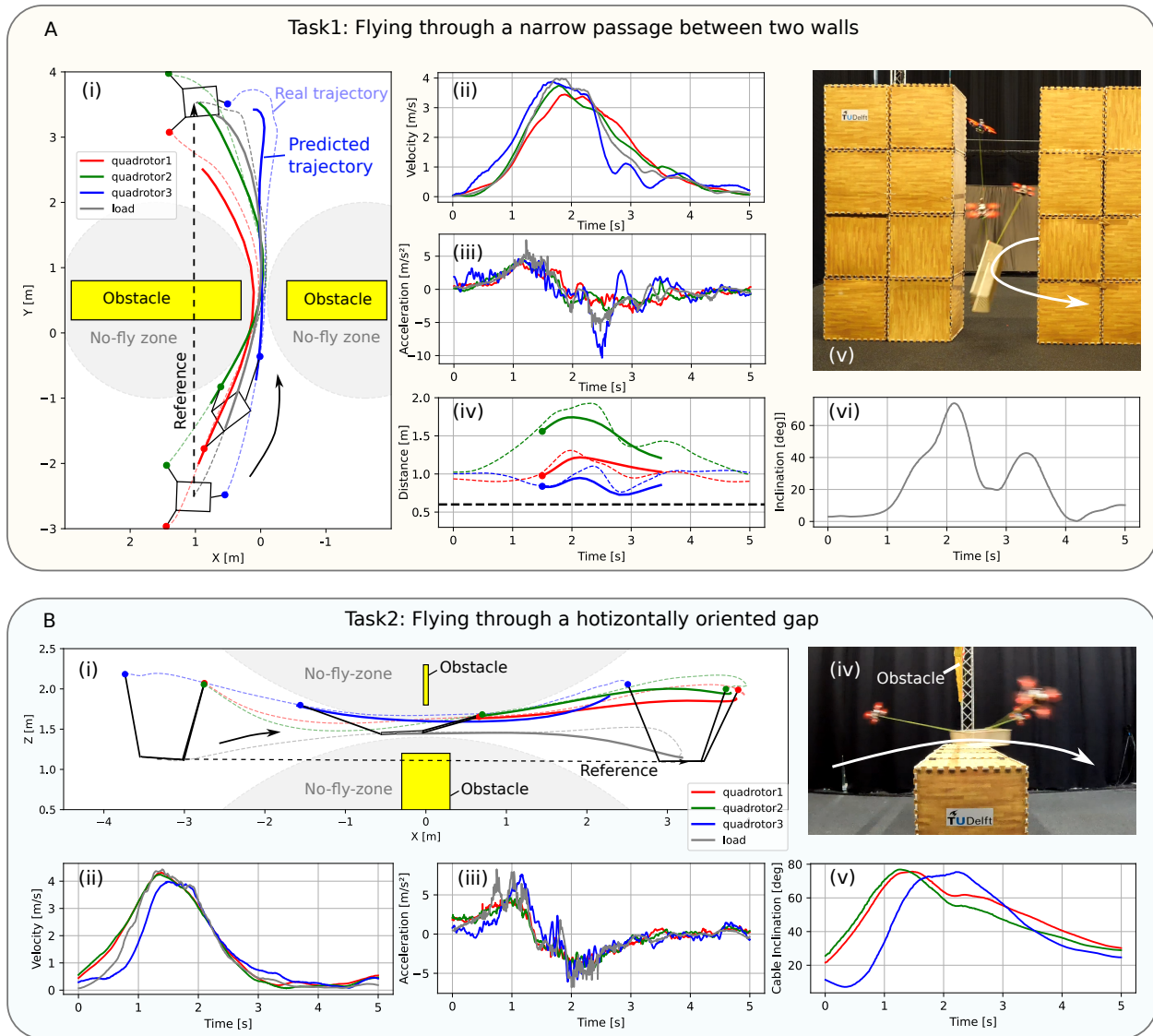


Figure 5: Obstacle avoidance through dynamic motion. Both tasks are provided with a line segment reference that originally collided with the obstacles. **(A)** Task 1: Flying through a narrow passage between two walls. (i) Top view shows the flight trajectory of the load center and three quadrotors (dash lines) with predicted trajectories (solid lines) at $t = 1.5$ s. The quadrotors dynamically carry the load through the narrow passage between two no-fly zones. (ii-iii) A top speed of over 4 m/s and acceleration of over 5 m/s² are achieved, leading a dynamic traversal. (iv) Quadrotors distances remain above the safety minimum of 0.6 m. (vi-v) Since the gap exceeds the load size, the load is controlled to incline by over 70 deg to pass through. **(B)** Task 2: Flying through a horizontally oriented narrow gap. (i) Side view of the trajectory and predicted trajectories generated at $t = 1.5$ s. (ii-iii) A top speed of over 4 m/s and top acceleration of over 8 m/s² has been achieved to gain sufficient momentum for a dynamic traversal. (iv-v) At the moment of traversal, all three cables are largely inclined (almost horizontal) because the gap is shorter than the cable length.

from the real obstacles. We select several reference points on the load, and each quadrotor. Then the algorithm ensures that none of these reference points enter the no-fly zones. Specifically, the reference points in this experiment are the center of each quadrotor and the four edges of the payload. At the same time, the error between the actual and the reference pose is minimized in the cost function, encouraging the system to continue moving toward the final target pose.

Fig. 5A presents the experimental data, illustrating the maneuvering process. Our proposed algorithm generates predicted trajectories for both the load and the quadrotors at 10 Hz, allowing them to fly through the gap while adhering to the dynamic model of the entire system. The planner automatically exploits the redundancy of the system to change the cable directions. Since the width of the load (0.54 m) is greater than the gap between two no-fly-zones 0.2 m, the quadrotors manage to steer the load at a steep inclination of approximately 70 deg to squeeze through the gap. The distances between quadrotors are also included as the constraints of the optimization problem. Hence their distances have been kept greater than a safe margin (0.8 m) through the traversal. Despite successfully avoiding the obstacles, the speed of the maneuver is not compromised. The system reaches a top speed of 4 m/s during the fly-through maneuver, with a peak acceleration of over 5 m/s². The load passes through the gap within 1.2 s from the start of the maneuver and eventually stabilizes at the target pose after successfully completing the traversal.

2.4.2 Flying through a horizontally orientated narrow gap

In the second task, the quadrotors need to carry the load to fly through a horizontally oriented gap with a height of 0.6 m, while the height of the multi-lifting system is around 1.2 m in hover. The experimental data of this fly-through motion is presented in Fig 5B. This time, we define two horizontal cylinders as no-fly zones, each with a radius of 4 m, ensuring that the two obstacles are encompassed within the no-fly zones with a minimum safety margin of 0.2 m. The load is initially controlled to hover. Next, a target pose behind the gap is sent to the algorithm, which generates a minimum snap reference trajectory. This trajectory intersects with one of the obstacles.

Since the vertical size of the gap between two no-fly zones is only 0.2 m, which is smaller than the height of the multi-lifting system in hovering conditions when all cables are nearly vertical (approximately 1.2 m), our algorithm controls the quadrotors to spread out and stretch the cables, reducing the total height of the system to enable it to fly through the gap. In this process, the directions of the cables rapidly changed from nearly vertical to almost horizontal within 1.2 s. At the moment of traversal when the cables are almost horizontal, the vertical components of the cable tensions cannot compensate for the gravity of the load. Therefore, the algorithm automatically leads to dynamic motions and takes advantage of the momentum of the system to fly through the gap. In this process, the load reaches a maximum velocity of 4 m/s, and a peak acceleration of over 7 m/s², generating the necessary momentum for a successful traversal.

2.5 Robustness

In this section, we demonstrate the robustness of our method in handling load dynamic model mismatches and addressing communication delays, which are inevitable in real-world operations. It is impractical to obtain a perfect dynamical model of the load, especially its inertia properties in real-world operations. The robustness is analyzed through simulation studies where the levels of model mismatch and communication delays can be controlled. Then, we also perform a case study in the real-world experiment, where we introduce a load with a time-varying inertia property (sloshing load).

2.5.1 Controlled experiments

We perform comparative studies against the benchmark geometric controller (13) in a simulation environment, where we can precisely quantify the level of model mismatch. The geometric controller also includes integral gains for both position and attitude control loops to address the model mismatch and disturbances. These mismatch types include mass variations, inertia, and the CoG offset. Apart from the model mismatch, the communication delay between the centralized controller (or planner in our solution) and quadrotors is also simulated to compare its effects on both methods.

We performed both trajectory tracking and setpoint tracking (constant reference) experiments under these conditions to evaluate performance. The reference trajectories are the same as listed in Table. 1, with a label *Slow*, *Medium*, and *Fast* respectively. The setpoint control task commands the load to move horizontally by 2 m and will change its roll, pitch, and yaw angles by 30 deg, 20 deg, and 90 deg respectively. We carefully tune the gains of the baseline geometric method in different tasks to achieve satisfactory accuracy and response time in the nominal conditions. Specifically, the gains for setpoint tracking are significantly smaller than the trajectory tracking to avoid oscillations. By contrast, our method’s control gains and weights remain consistent across different tasks and trajectories.

Fig. 6 presents the position and attitude tracking error of the geometric controller and our method. Since the geometric controller failed to track fast trajectory even under nominal conditions, we only show its tracking performance for trajectory *Slow* and *Medium*. As is shown in the box plots of Fig. 6, the benchmark controller, despite adding integral gains, is more sensitive to the model mismatch, especially on attitude control. By contrast, our approach can sustain an over 50% mass and inertial mismatch in all the tests. These inertial model mismatches do not degrade the tracking performance even tracking the fastest reference trajectory with a maximum velocity of 5 m/s and a maximum acceleration of 8 m/s². Only the case with a 10% bias of CoG will lead to an increase in attitude tracking error of about 5 deg.

The benchmark method is sensitive to inertial model mismatch because it relies on a force-control scheme that requires an accurate inertial model to generate the desired force vector for each

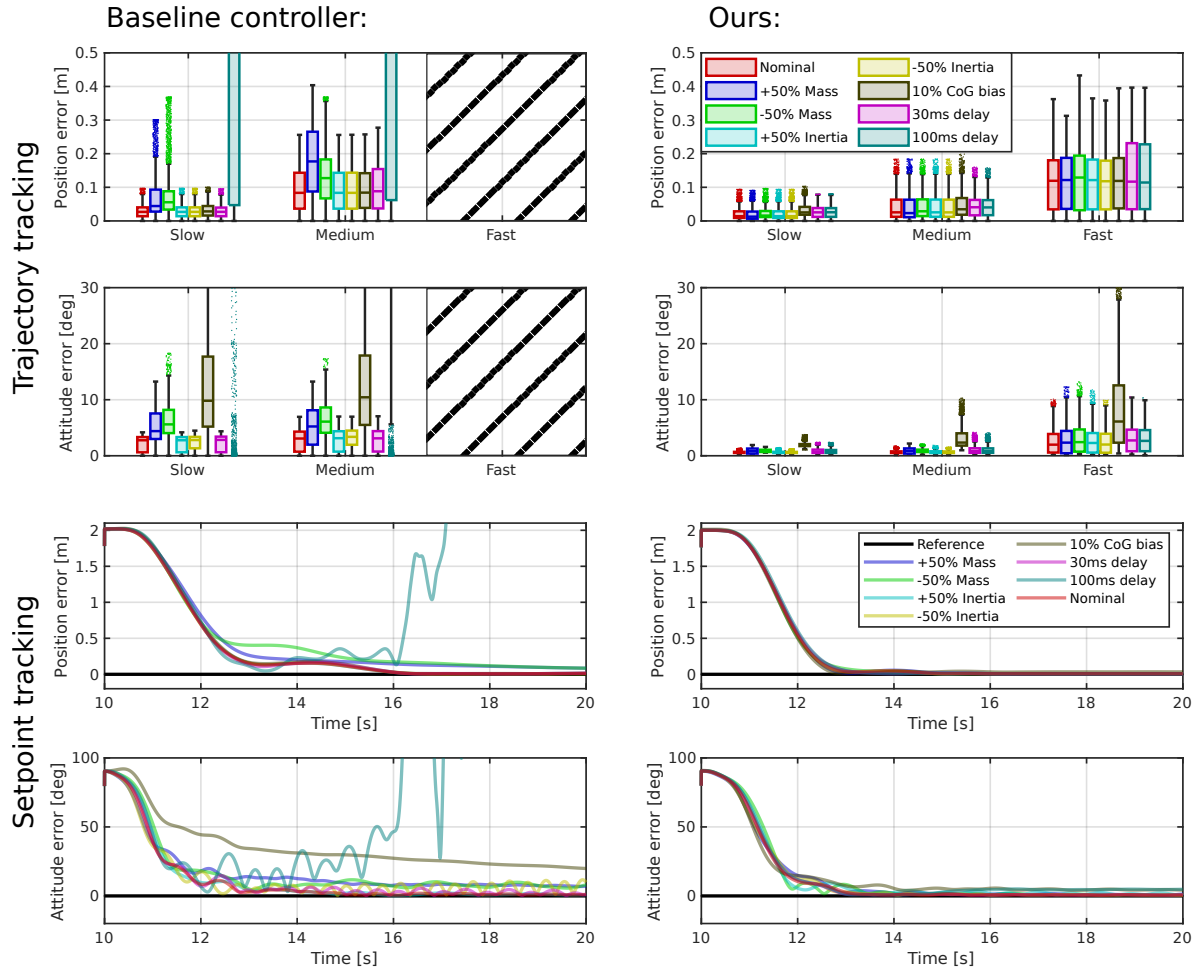


Figure 6: Robustness test results. The results are obtained in a controlled simulation environment to introduce different levels of inertia model mismatch and communication delay. **(Left)** The baseline controller (geometric controller with integral controls (13)) generates the force command of each quadrotor, being sensitive to the inertia model mismatch of the load. Note that the baseline controller failed to track reference *Fast* even under nominal conditions. **(Right)** our method, which does not generate force command but a reference trajectory, is robust against inertia model mismatch of the load, and communication delay of 100 ms, even while tracking the reference *Fast*.

quadrotor. Therefore, any modeling error in the inertial properties will lead to erroneous attitude and thrust command of quadrotors. On the other hand, our method adopts a trajectory-based control scheme. Instead of solely producing a desired force, our method also generates reference trajectories for the quadrotors online. Hence the tension error of each cable, due to the load model mismatch, will be reflected as an external disturbance acting on each quadrotor, which can be compensated by a disturbance rejection controller deployed onboard.

Moreover, sending reference trajectories to quadrotors instead of single reference points also offers significantly higher robustness communication delays. Under a delay of 100 ms, the benchmark method loses effectiveness, whereas our method remains unaffected. Additional results comparing the tracking performance of our method and the benchmark method under varying levels of delay between the centralized controller and the quadrotors are presented in Fig. 7.

2.5.2 Case study: unknown sloshing load

We chose a challenging case study to demonstrate the performance of our controller under dynamic uncertainties in real-world experiments. In this experiment, we place a 0.6 kg-weight basketball into the original basket-shaped load to introduce the sloshing motion, which can freely move in the original payload (Fig. 8). Note that this leads to a mass mismatch of 43% given the mass of the original load is 1.4 kg. The movement of the basketball during flight also results in a significant, time-varying mismatch in the CoG and inertia of the load, if we consider the basketball and the original load as a single unit. On the other hand, we do not modify any parameters in the algorithm; the presence of the basketball is entirely unknown to our method. Despite that, we still let the multi-lifting system follow the trajectory *Fast* as listed in Table. 1. The snapshot of the system with sloshing load and the trajectory tracking results are presented in Fig. 8.

Since the multi-lifting system in this experiment consists of only three quadrotors, each connected to the load by a single cable, it is not in force closure and thus cannot generate an arbitrary wrench to counteract a disturbance wrench (19). Therefore, the sloshing inevitably induces additional swaying motions, particularly while conducting dynamic motions. We observe higher tracking errors in certain instances, particularly in attitude tracking. For example, at $t = 26$ s, the basketball's position rapidly shifts inside the basket, generating an impact torque on the load and causing an unintended yawing motion. Consequently, the tracking error is slightly larger after adding a sloshing load (0.216 m vs 0.193 m for position RMSE and 16 deg vs. 11.1 deg for attitude). Nevertheless, our algorithm manages to control the multi-lifting system to follow the reference *Fast* with an unknown sloshing load, which cannot be successfully achieved by benchmark methods even with a perfect model (see Table 1).

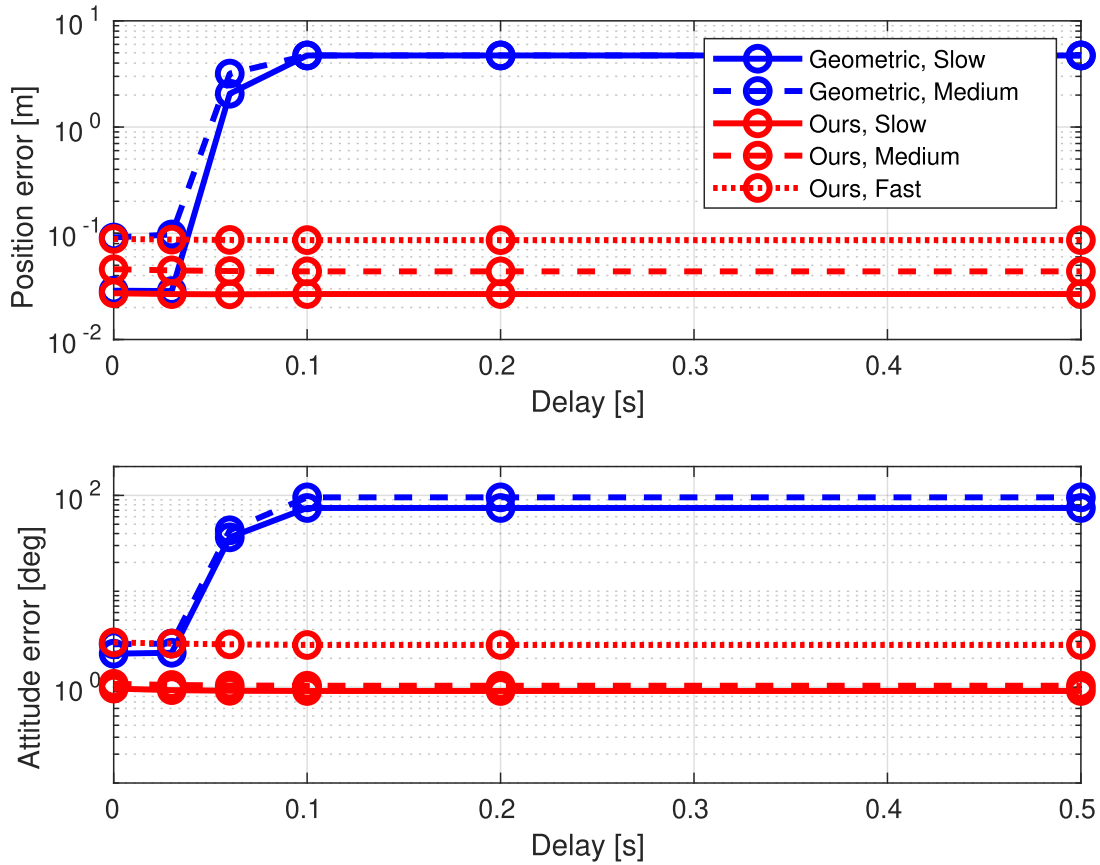


Figure 7: Results of delay analysis. We simulate the communication delay between the centralized controller (the planner in our case) and the quadrotors. The position and attitude errors are compared between our method and the benchmark geometric controller for tracking different trajectories (*Slow*, *Medium*, *Fast*, as defined in Table 1). While the benchmark method can only tolerate delays of up to approximately 30 ms, our method remains unaffected by communication delays and performs effectively even with a delay of 0.5 s.

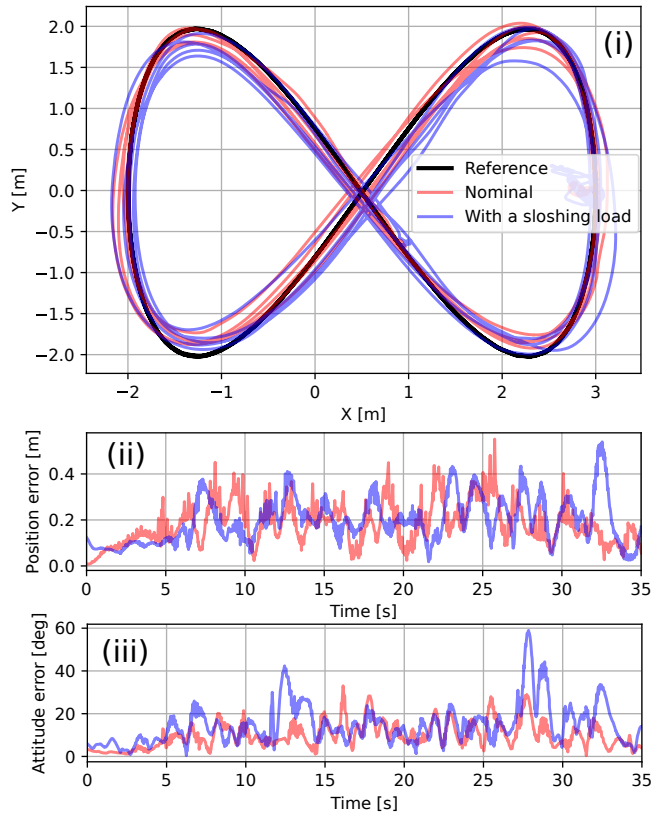
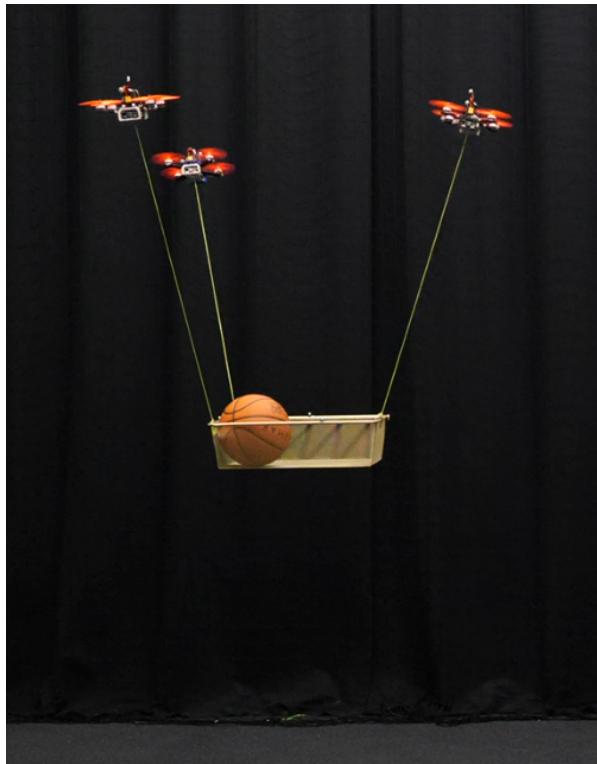


Figure 8: Trajectory tracking with a sloshing load. (Left) A snapshot of the experiment, where a 0.6 kg basketball is placed onto the 1.4 kg basket-shaped load, introducing significant inertia model mismatch for the entire load. Our algorithm runs without knowing the presence of the basketball. (Right) (i) Top view of the trajectory tracking performance with and without adding the basketball. (ii-iii) Time history of the position error and attitude error.

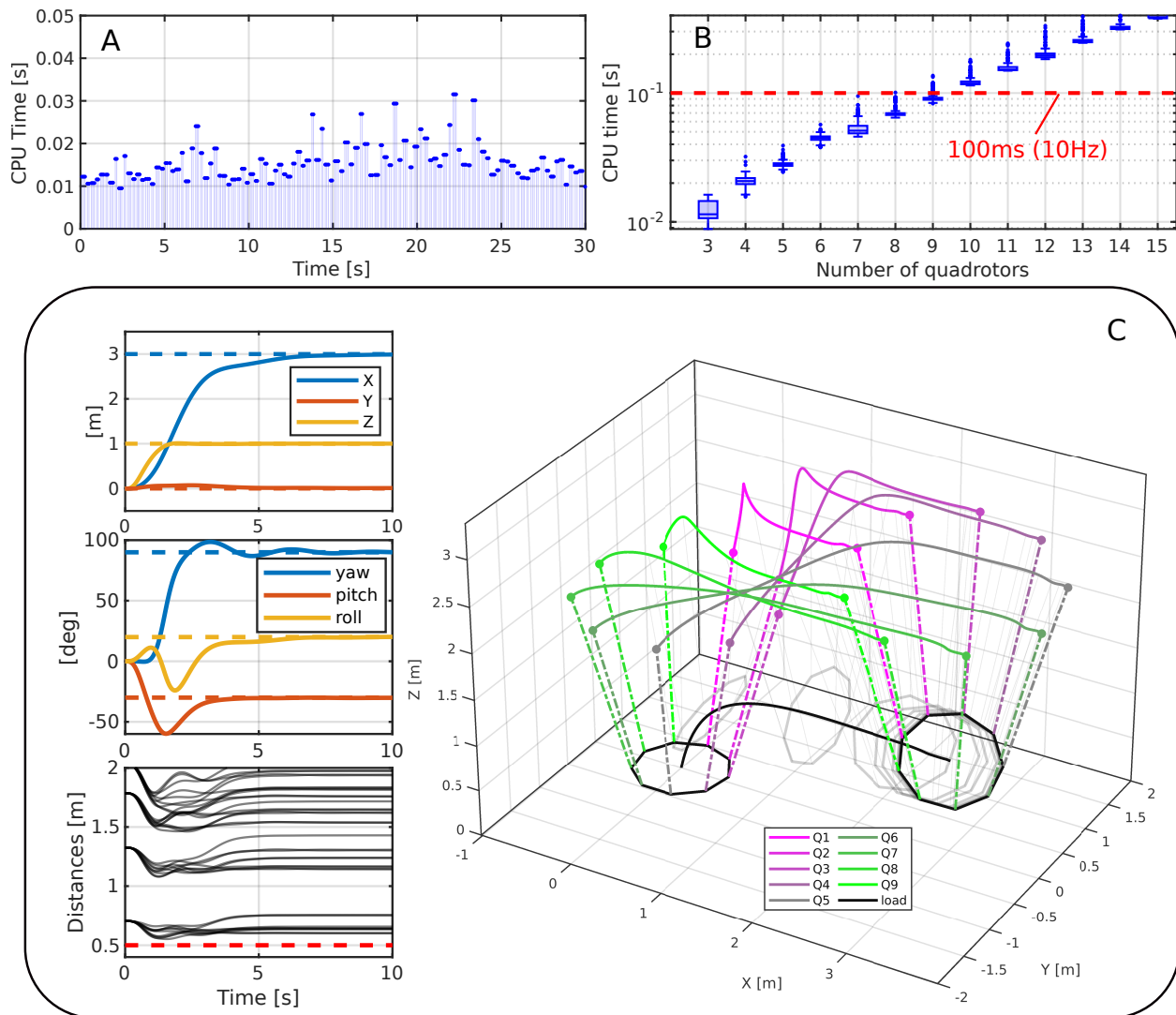


Figure 9: Computational load and scalability. (A) The CPU time to solve each OCP to follow the reference trajectory *Fast* with 3 quadrotors in real-world experiments. (B) Box plot of the CPU time of planning a trajectory with different numbers of quadrotors in a setpoint control task. (C) The 3D plot, position and orientation tracking, and distances between quadrotors in a task including 9 quadrotors.

2.6 Computational Load and Scalability

Our method utilizes a centralized structure, aiming at reaching optimality to coordinate all the agents to manipulate the payload. The centralized structure, particularly the planner, brings a challenge to run in real-time while multiple quadrotors are involved. The real-world experiments have demonstrated that our method can successfully coordinate at least 3 units in real-time. Fig. 9A presents the CPU time of the laptop running the planner (Intel Core i7-13700H) while performing tracking the trajectory *Fast*. The average CPU time that the planner consumes is 15.3 ms. Since the planner runs at 10 Hz, namely every 100 ms, our algorithm only takes 15.3% of the computational budget.

Therefore, we explore the potential of scaling up our algorithm to include more units. We conduct experiments in the simulation environment to perform a setpoint tracking task with more quadrotors involved. Without loss of generality, we assume the load is centrosymmetric, and the cables are connecting to points evenly distributed around the load center at equal angular intervals that depend on the number of quadrotors involved. The mass of the load is scaled up as the number of the quadrotors grows. We set the minimum distance constraint between quadrotors to be 1.6 times the distance between the corresponding contact points on the load, ensuring that there remains a possibility of violating the constraint if it is not imposed. As a result, Fig. 9B indicates that CPU time exponentially grows as the number of quadrotors is included in the system. With our hardware setup, the planner in our proposed framework can include up to nine units before fully taking up the computational budget to run the planner at 10 Hz. Fig. 9C presents the simulation results with nine quadrotors, including the pose tracking result, distances between quadrotors, and a 3D-space illustration. We believe that with a tailored optimizer to this particular problem, and other software/hardware optimization, our method can be scaled up to significantly more units.

3 Discussion

Our experiments show that the proposed trajectory-based framework can significantly enhance the agility, robustness, and practicality of cable-suspended multi-lifting systems compared to the state-of-the-art. To consider the dynamic coupling effects, the state-of-the-art framework requires a cascaded structure to coordinate and control multiple quadrotors to collaborate. This conventional structure is built upon the principle of time-scale separation, assuming that quadrotors can instantly generate a resultant wrench on the load requested by an outer-loop controller, which limits the outer-loop gains to prevent instability and make the tuning process tedious and task-specific (15). Consequently, agility (high gain) and safety (low gain) are considered contradictory in the traditional framework.

In contrast, our method does not require the cascaded structure and addresses this issue by

solving an online kinodynamic planning problem that considers the whole-body dynamics of the load-multi-quadrotor system. The solution generates the states of the system over a future horizon, offering a predictive capability that allows for the inclusion of safety constraints during agile motion, rather than simply limiting gains in the traditional framework. This key component of our solution enables precise pose control, trajectory tracking, and obstacle avoidance at high speeds (over 5 m/s) and accelerations (over 8 m/s²). Although the kinodynamic motion planning accounts for the whole-body dynamics, we have demonstrated that this problem is solvable on a midrange CPU in just a few milliseconds, enabling fast online generation to adjust to disturbances and avoid obstacles. The CPU time of the planner increases almost exponentially with the number of quadrotors included in the problem. Our benchmarking results demonstrate that our method can scale up to nine units with the current hardware and software setup, which is sufficient for a wide range of applications.

We send the predicted trajectories to each quadrotor instead of a single reference point, offering two major advantages. First, by deploying a reference sampler and a robust trajectory tracking controller on the quadrotors, our framework significantly more robustness against communication delay and inertia model mismatch of the load. Although the planner requires the model of the load, the mismatch of its inertia will be reflected as an external force on the quadrotor, which can be compensated for by the robust trajectory tracking controller onboard. This enables our algorithm to safely control the cable-suspended multi-lifting system, even when handling an unknown-mass sloshing load that brings over 40% mismatch on the load mass model. Second, sending a trajectory allows us to run the planner at a significantly lower frequency than traditional controllers, reducing computational load and, more importantly, eliminating the need for external sensors on the load to provide high-frequency measurements. Instead, a simple yet effective state estimator can be used to supply the planner with state estimates, without requiring additional sensors.

We see several opportunities for future work. Beyond the quadrotor multi-lifting problem, the trajectory-based framework has the potential to be applied to a wider range of robotic collaboration challenges, particularly those involving dynamic coupling, agility, and safety constraints. Despite that our method guarantees high accuracy in the presence of load mismatch, an underestimation of the load mass and inertia may cause the violation of maximum thrust constraints. This problem can be alleviated by estimating the inertial properties online (30), or employing the constrained tightening technique employed by robust nonlinear optimal control framework, such as robust MPC (31, 32). This requires a pre-estimation of the uncertainties and provides a more conservative, yet safer reference for quadrotors to avoid any violation of its dynamical constraints. Another opportunity is the state estimation in the field. Despite that proving effective in real-world experiments, our algorithms are still validated in a well-controlled lab environment with the help of a motion capture system to provide pose measurements of quadrotors at 100 Hz. Future work needs to be performed to investigate the performance with estimators typically applied in outdoor environments, such as

the combination of GNSS/IMU, or visual-inertial-navigation system, and analyze their performance in the presence of cable tensions acting on the quadrotors. Wind disturbances are another challenge that needs to be addressed. Similarly to nonlinear predictive control for a single quadrotor, the wind effect will cause tracking errors. A disturbance observer can be further developed and combined with the proposed framework to compensate for the wind disturbances.

Thus, this work paves the way for aerial manipulation systems with significantly higher resilience, versatility, and agility to perform complex collaborative tasks in day-to-day operations, from search and rescue to precision delivery in difficult terrains.

4 Materials and Methods

An overview of the method is shown in Fig. 10. Our method incorporates an optimization-based kinodynamic motion planner that generates references for quadrotors in real time. Onboard each quadrotor, a time-based sampler and a trajectory tracking controller based on INDI are implemented. The framework also includes a centralized EKF to estimate the load pose and cable directions based on the position, velocity, and IMU measurements of the quadrotors. All these modules are model-based and rely on a dynamic model of the cable-suspended multi-lifting system. The following sections provide a detailed introduction to each module.

4.1 Modeling of cable-suspended multi-lifting systems

4.1.1 Load-cable dynamic model

The load-cable dynamic model describes the 6-DoF motion of the load, as well as motion of all the cables attached to the load. Specifically, the state of the load-cable kinodynamic model includes

$$\mathbf{x} = [\mathbf{p}, \mathbf{v}, \mathbf{q}, \boldsymbol{\omega}, \mathbf{s}_1, \mathbf{r}_1, \dot{\mathbf{r}}_1, \ddot{\mathbf{r}}_1, t_1, \dot{t}_1, \dots, \mathbf{s}_n, \mathbf{r}_n, \dot{\mathbf{r}}_n, \ddot{\mathbf{r}}_n, t_n, \dot{t}_n] \quad (1)$$

where n is the number of quadrotors, $\mathbf{p} \in \mathbb{R}^3$, $\mathbf{v} \in \mathbb{R}^3$ are position and velocity of the load, $\mathbf{q} \in \mathbb{S}^3$ is the unit quaternion describing the load attitude, $\boldsymbol{\omega} \in \mathbb{R}^3$ is the load angular velocity expressed on the load-fixed coordinate frame \mathcal{F}_L . We use subscript i for variables of the cable connected to the i -th quadrotor, where $\mathbf{s}_i \in \mathbb{S}^2$ is the cable direction pointing from the quadrotor to the load, $\mathbf{r}_i \in \mathbb{R}^3$ is the cable angular velocity, $t_i \in \mathbb{R}$ is the cable tension. An illustration of the reference frames and some symbols defined above can be found in Fig. 11.

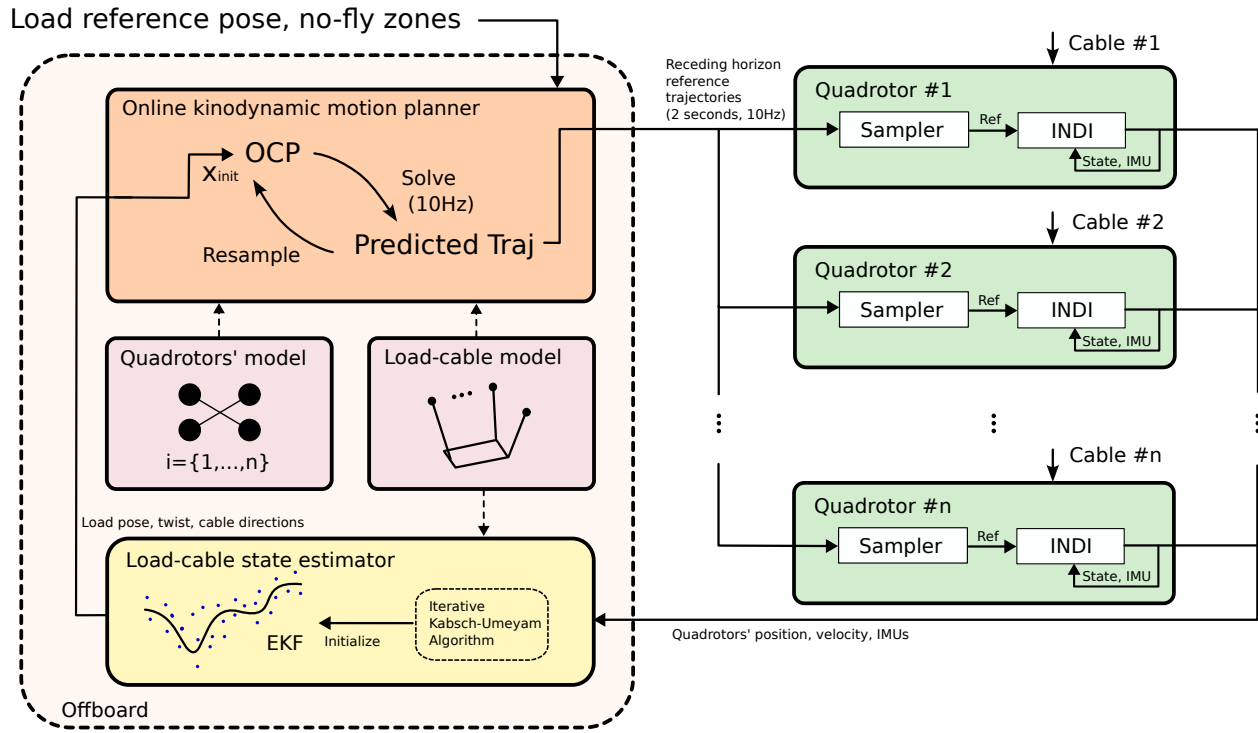


Figure 10: Method overview. A kinodynamic motion planner solves an OCP online at 10 Hz to generate receding-horizon reference trajectories of quadrotors given load reference pose and pre-defined no-fly zones. The OCP utilizes the whole-body dynamics of the system, including the quadrotors model and the load-cable model. The load’s pose and twist and cable directions are obtained from an EKF-based estimator. The remaining elements in the initial state of the OCP, namely the derivatives of the cable directions and tensions, are obtained by resampling the previously generated predicted trajectory to avoid jittery motions of the quadrotor when a new reference is received. The load state estimator fuses the load-cable model, and the quadrotors’ position, velocity, and IMU measurements to obtain estimates of load pose, twist, and cable directions. It is initialized through an iterative Kabsch-Umeyam algorithm given the initial quadrotor states. Onboard each quadrotor, a time-based sampler samples the received receding horizon reference trajectory using the current timestamp to generate a single reference point which is tracked by a trajectory tracking controller based on the incremental nonlinear dynamic inversion (INDI) technique that regards the cable tensions as external disturbances, and compensates for them using the IMU measurements.

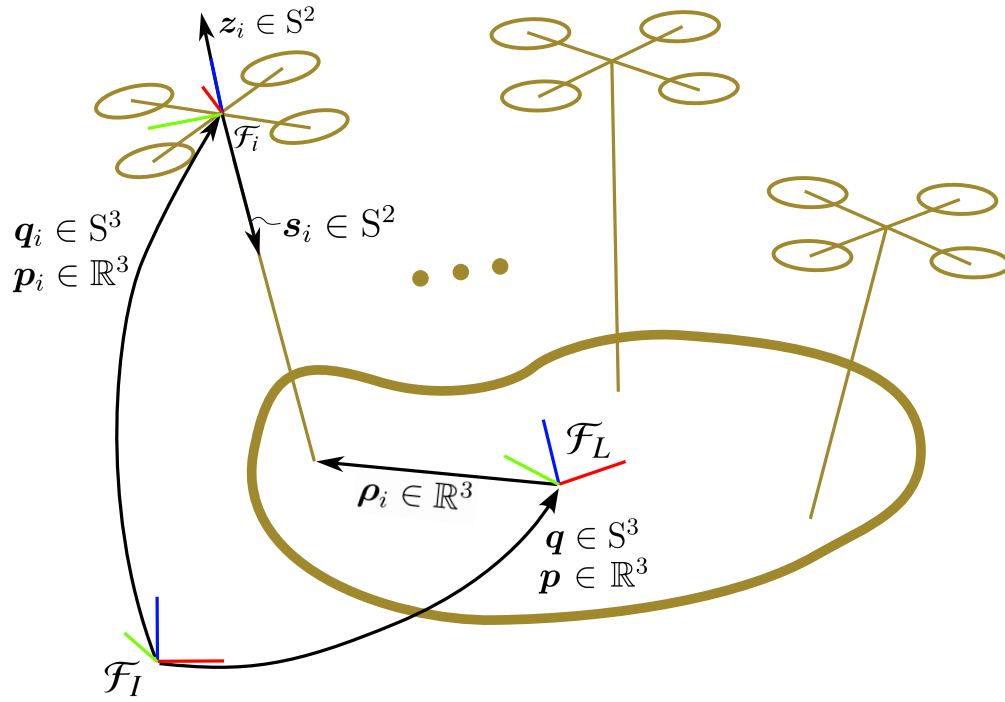


Figure 11: Definition of reference frames and symbols. \mathcal{F}_I , \mathcal{F}_L , \mathcal{F}_i respectively denotes the inertial frame, load-fixed frame, and the i -th quadrotor-fixed frame, where the x , y , z are marked in red, green, blue colors respectively.

The dynamic equations of the load can be written down as

$$\begin{aligned}
\dot{\mathbf{p}} &= \mathbf{v}, & \dot{\mathbf{v}} &= -\sum_{i=1}^n t_i \mathbf{s}_i / m + \mathbf{g}, \\
\dot{\mathbf{q}} &= \frac{1}{2} \mathbf{\Lambda}(\mathbf{q}) \begin{bmatrix} 0 \\ \boldsymbol{\omega} \end{bmatrix} \\
\mathbf{J} \dot{\boldsymbol{\omega}} &= -\boldsymbol{\omega} \times \mathbf{J} \boldsymbol{\omega} + \sum_{i=1}^n t_i (\mathbf{R}(\mathbf{q})^\top \mathbf{s}_i \times \boldsymbol{\rho}_i)
\end{aligned} \tag{2}$$

where $\mathbf{J} \in \mathbb{R}^{3 \times 3}$ is the load inertia, m is the load mass, $\boldsymbol{\rho}_i \in \mathbb{R}^3$ is the displacement of the i -th attachment point, expressed in the load frame, and $\mathbf{g} = [0, 0, -9.81 \text{m/s}^2]^\top$ is the gravity vector. $\mathbf{\Lambda}(\mathbf{q})$ represents a quaternion multiplication, $\mathbf{R}(\mathbf{q})$ is the quaternion rotation. To ensure smoothness in the quadrotor reference to the jerk level, the cable kinematic equations take the 3rd-order derivative of cable angular velocity, and the 2nd-order derivative of cable thrust as bounded input, yielding

$$\dot{\mathbf{s}}_i = \boldsymbol{\gamma}_i \times \mathbf{s}_i, \quad \ddot{\mathbf{r}}_i = \boldsymbol{\gamma}_i, \quad \ddot{t}_i = \lambda_i, \quad \text{where } i = \{1, \dots, n\} \tag{3}$$

where $\boldsymbol{\gamma}_i \in \mathbb{R}^3$ can be the snap of cable directions, and λ_i is the second-order derivative of cable tensions. In the Appendix, we prove that the generated quadrotor trajectories are smooth up to the jerk level and also lead to a smooth angular velocity reference by choosing states for the cable-load kinodynamic model in Equation 1, as long as the $\boldsymbol{\gamma}_i$ and λ_i are bounded.

4.1.2 Quadrotor dynamic model

The quadrotor dynamics is established using standard rigid body dynamics (33). For the i -th quadrotor, the state space is described as $\mathbf{x}_i = [\mathbf{p}_i, \mathbf{v}_i, \mathbf{q}_i, \boldsymbol{\omega}_i]$, which corresponds to the CoG position $\mathbf{p}_i \in \mathbb{R}^3$, velocity $\mathbf{v}_i \in \mathbb{R}^3$, unit quaternion rotation $\mathbf{q}_i \in \mathbb{S}^3$, and angular velocity of expressed in the quadrotor fixed coordinate system $\boldsymbol{\omega}_i \in \mathbb{R}^3$. The dynamic equations are

$$\begin{aligned}
\dot{\mathbf{p}}_i &= \mathbf{v}_i, & \dot{\mathbf{v}}_i &= (T_i \mathbf{z}_i + t_i \mathbf{s}_i + \mathbf{f}_{a,i}) / m_i + \mathbf{g} \\
\dot{\mathbf{q}}_i &= \frac{1}{2} \mathbf{\Lambda}(\mathbf{q}_i) \begin{bmatrix} 0 \\ \boldsymbol{\omega}_i \end{bmatrix} \\
\mathbf{J}_i \dot{\boldsymbol{\omega}}_i &= -\boldsymbol{\omega}_i \times \mathbf{J}_i \boldsymbol{\omega}_i + \boldsymbol{\tau}_i + \boldsymbol{\tau}_{a,i}
\end{aligned} \tag{4}$$

where m_i and $\mathbf{J}_i \in \mathbb{R}^{3 \times 3}$ are respectively the mass and the inertia of the i -th quadrotor; T_i is the collective thrust; $\mathbf{z}_i \in \mathbb{S}^2$ is the thrust direction, typically aligns with the z axis of the quadrotor body-fixed frame \mathcal{F}_i ; $\mathbf{f}_{a,i} \in \mathbb{R}^3$ and $\boldsymbol{\tau}_{a,i} \in \mathbb{R}^3$ are the aerodynamic drag force and moment; $\boldsymbol{\tau}_i \in \mathbb{R}^3$ is the control torque generated by the rotors.

4.1.3 Kinematic constraints

We assume the tautness of the cables is maintained by our algorithm throughout the operation, even during agile motions. On the i -th quadrotor, we denote the position of the cable contact point in the inertial frame as $\hat{\mathbf{p}}_i$. Then, the following kinematic constraint between the i -th quadrotor and load-cable dynamics holds

$$\mathbf{p}_i = \mathbf{p} + \mathbf{R}(\mathbf{q})\boldsymbol{\rho}_i - l_i \mathbf{s}_i \quad (5)$$

where l_i is the length of the cable.

4.2 Online kinodynamic motion planner

4.2.1 Finite-time optimal control problem

Our framework includes a centralized kinodynamic motion planner that generates smooth reference trajectories of all quadrotors in a receding horizon fashion while considering the dynamic coupling between load and quadrotors. Specifically, the planner is a discretized finite-time OCP, solved by a multi-shooting method (34)

$$\begin{aligned} \min J = & \sum_{k=0}^{N-1} \left(\|\mathbf{x}_k - \mathbf{x}_{k,\text{ref}}\|_{\mathbf{Q}}^2 + \|\mathbf{u}_k - \mathbf{u}_{k,\text{ref}}\|_{\mathbf{R}}^2 \right) \\ & + \|\mathbf{x}_N - \mathbf{x}_{N,\text{ref}}\|_{\mathbf{P}}^2 \end{aligned} \quad (6)$$

$$\begin{aligned} \text{subject to} \quad & \mathbf{x}_0 = \mathbf{x}_{\text{init}}, \quad \mathbf{x}_{k+1} = f(\mathbf{x}_k, \mathbf{u}_k) \\ & \mathbf{h}(\mathbf{x}_{k+1}, \mathbf{u}_k) \leq \mathbf{0}, \quad k \in \{0, \dots, N\} \end{aligned}$$

where the state equation uses the load-cable dynamic model (Equation 2 and 3), and the input is $\mathbf{u} = [\boldsymbol{\gamma}_1, \lambda_1, \dots, \boldsymbol{\gamma}_n, \lambda_n]$. $\mathbf{u} = [\ddot{\mathbf{r}}_1, \dot{t}_1, \dots, \ddot{\mathbf{r}}_n, \dot{t}_n]$. The quadrotor dynamics, albeit not explicitly included in the state equation for the reason of numerical efficiency, are included in the path constraints particularly to avoid overloading quadrotors, and to perform obstacle avoidance.

The cost function is in a standard quadratic form to minimize the load pose tracking error and control effort for smoothness. The reference states used in the cost function of the OCP are precomputed based on a polynomial load pose reference, with the remaining states derived using the flatness property of the cable-suspended multi-lifting system (9). It is worth noting that in our experiments, the load reference does not consider avoiding obstacles. Instead, we leave the planner to decide and generate commands for quadrotors to carry the load to avoid the obstacles. In other words, the planner has the flexibility to deviate from the reference position or adjust the configurations to satisfy the obstacle avoidance constraints. Naturally, our method can also follow load references generated by a higher-level offline planner (e.g., (16)), other than the simple polynomial reference.

We discretize the horizon into $N = 20$ non-equidistant segments, with intervals linearly increasing along the horizon. Hence, it ensures higher fidelity of the predicted trajectory in the near future while extending the horizon length without increasing the number of discretization nodes. This OCP is subsequently solved through sequential quadratic programming (SQP) algorithm in a real-time iteration (RTI) scheme (35), implemented using ACADOS toolkit (36). The solution of the OCP is the optimal input \mathbf{u}_k^* and load-cable state \mathbf{x}_k^* along the horizon

$$\begin{aligned} \mathbf{U}^* &= [\mathbf{u}_0^*, \mathbf{u}_2^*, \dots, \mathbf{u}_{N-1}^*], \\ \mathbf{X}^* &= [\mathbf{x}_1^*, \mathbf{x}_2^*, \dots, \mathbf{x}_N^*] = \boldsymbol{\pi}(\mathbf{U}^*, \mathbf{x}_{\text{init}}) \end{aligned} \quad (7)$$

Once the optimal state sequence \mathbf{X}^* has been calculated, we convert them to the position, velocity, acceleration, and jerk of the quadrotor through kinematic constraints (Equation 5) and its derivatives. It is worth noting that the headings of quadrotors, defined as the rotation angle around \mathbf{z}_i , do not affect the thrust directions or the motion of the load. Therefore, we avoid explicitly setting the heading reference for the quadrotors but let the quadrotors maintain a zero yaw rate instead.

The OCP is solved at a fixed frequency to generate a new trajectory online. The initial state \mathbf{x}_{init} in OCP is provided partially by the load-cable state estimator (Section 4.3), and partially by resampling the trajectory generated in the last step. Specifically, we take the estimated load pose, twist, and cable directions to renew \mathbf{x}_{init} to make sure the trajectories take the up-to-date state of the load for closed-loop control. The other states (cable rate, cable tensions, and their high-order derivatives) are directly estimated by resampling on the previously generated trajectory. We observe that this treatment ensures smooth transitions between consecutive reference trajectories, avoiding any abrupt and jerky maneuvers by the quadrotors.

4.2.2 Path constraints

We define several path constraints $\mathbf{h}(\mathbf{x}) \leq \mathbf{0}$ in the OCP to ensure safety. To avoid overloading each quadrotor, we include the thrust constraint

$$T_{i,\min} \leq T_i(\mathbf{x}) \leq T_{i,\max} \quad (8)$$

where $T_i(\mathbf{x})$ is the thrust of each quadrotor as a function of the state of the load-cable dynamic model. Specifically, $T_i(\mathbf{x})$ is obtained through quadrotor dynamics (Equation 4),

$$T_i(\mathbf{x}) = \left\| (\dot{\mathbf{v}}_i(\mathbf{x}) - \mathbf{g}) m_i - t_i \mathbf{s}_i - \mathbf{f}_{a,i} \right\| \quad (9)$$

where $\dot{\mathbf{v}}_i(\mathbf{x})$ is calculated from the second-order derivative of the kinematic constraints (Equation 5).

Our algorithm assumes that the cables remain taut throughout the operation; therefore, a cable tension constraint is incorporated.

$$0 < t_{\min} \leq t_i \leq t_{\max} \quad (10)$$

To avoid internal collision between quadrotors, the minimum distance constraints are also provided for every pair of quadrotors indexed by i and j

$$0 < d_{\min} \leq \|\mathbf{p}_i(\mathbf{x}) - \mathbf{p}_j(\mathbf{x})\| \quad (11)$$

where d_{\min} is the pre-defined minimum distance, $\mathbf{p}_i(\mathbf{x})$ and $\mathbf{p}_j(\mathbf{x})$ are the positions of the i -th and the j -th quadrotor.

We also establish several control points on the system to ensure it avoids obstacles. Without loss of generalizability, we use the CoG of each quadrotor together with the attaching points on the load as the control points. For each obstacle, and each control point denoted by $\mathbf{p}_c(\mathbf{x})$, the following constraint ensures that none of the control points enters the no-fly zone encompassing the obstacle

$$d_{o,\min}^2 \leq (\mathbf{p}_c(\mathbf{x}) - \mathbf{p}_o)^\top \mathbf{C} (\mathbf{p}_c(\mathbf{x}) - \mathbf{p}_o) \quad (12)$$

where $\mathbf{C} \in \mathbb{R}^{3 \times 3}$ is a diagonal matrix controlling the shape of the no-fly-zone, \mathbf{p}_o is the center of the no-fly zone, $d_{o,\min}$ is the safe distance from the control points to the center. We assume the position and shape of the obstacle are known, and the no-fly zone is also determined offline.

Lastly, to ensure the bounded input to the OCP, the control input constraint $\mathbf{u}_{\min} \leq \mathbf{u} \leq \mathbf{u}_{\max}$ is imposed.

It is worth noting that all path constraints are inequality constraints and are handled using slack variables to ensure solver feasibility.

4.3 Load-cable state estimator

To update \mathbf{x}_{init} in the OCP of the planner, the load pose, twist, and cable directions must be estimated in real-time. Instead of relying on additional sensors such as downward facing camera (10) or adding motion capture markers on the load (22) in the state-of-the-art approaches, our proposed estimator utilizes only the accelerometer data from the IMU on each quadrotor and the load-cable dynamics. This eliminates the need for any hardware modifications.

We choose EKF to solve this state estimation problem thanks to its simplicity and computational efficiency. We omit the detailed steps in EKF and only describe the selections of states, measurements, models, and initialization.

The EKF runs in a centralized fashion. It uses the load pose and twist, together with the position and velocities of all quadrotors as the state, namely $\hat{\mathbf{x}} = [\mathbf{p}, \mathbf{v}, \mathbf{q}, \boldsymbol{\omega}, \mathbf{p}_1, \mathbf{v}_1, \dots, \mathbf{p}_n, \mathbf{v}_n]$. Then, it uses the load dynamics and quadrotor dynamics (Equations 2 and 4) for state prediction. The cable directions to solve load dynamic is obtained through kinematic constraint (Equation 5). The cable forces in these equations are estimated through a spring-damper model, i.e., $t_i = k_{\text{stiff}}d_i + k_{\text{damp}}\dot{d}_i$ where d_i is the distance between the position of the i -th quadrotor and its connection point on the load, namely $d_i = \|\mathbf{p}_i - \mathbf{R}(\mathbf{q})\boldsymbol{\rho}_i - \mathbf{p}\|$.

The EKF takes the cable directions and quadrotors' positions and velocities as measurements, namely $\tilde{\mathbf{y}} = [\tilde{\mathbf{s}}_1, \tilde{\mathbf{p}}_1, \tilde{\mathbf{v}}_1, \dots, \tilde{\mathbf{s}}_n, \tilde{\mathbf{p}}_n, \tilde{\mathbf{v}}_n]$. The quadrotor positions and velocities and their covariances can be obtained directly from their onboard state estimators. The cable directions are obtained indirectly from the accelerometer sensor that is generally available on any quadrotor. Since the accelerometer directly measures the specific force (the mass-normalized force excluding gravity), it captures the combined forces, including the cable tension, aerodynamic drag, and rotor thrusts. For each quadrotor, we can identify a collective thrust model \bar{T}_i , and a drag model $\bar{\mathbf{f}}_{a,i}$

$$\bar{T}_i = \sum_{j=1}^4 c_t \omega_{j,i}^2, \quad \bar{\mathbf{f}}_{a,i} = \mathbf{R}(\mathbf{q}_i) \mathbf{D}_a \mathbf{R}(\mathbf{q}_i)^\top \mathbf{v}_i \quad (13)$$

where c_t is the thrust coefficient of the rotors, $\omega_{j,i}$ is the rotor speed, $\mathbf{D}_a \in \mathbb{R}^{3 \times 3}$ is the aerodynamic coefficient matrix (37). According to the quadrotor dynamics (Equation 4), subtracting them from the accelerometer readings provides the force vector from cables. Then the cable direction can be approximated by

$$\tilde{\mathbf{s}}_i = (m_i \mathbf{a}_i - \bar{T}_i \mathbf{z}_i - \bar{\mathbf{f}}_{a,i}) / \|m_i \mathbf{a}_i - \bar{T}_i \mathbf{z}_i - \bar{\mathbf{f}}_{a,i}\| \quad (14)$$

where $\mathbf{a}_i = \dot{\mathbf{v}} - \mathbf{g}$ is the unbiased accelerometer measurement.

We observe that the covariance matrix of the cable direction is challenging to determine directly from the accelerometer properties, as it also depends on the precision of the quadrotor model \bar{T}_i and $\bar{\mathbf{f}}_{a,i}$. Therefore, we tune this covariance experimentally. Underestimating the covariance can result in a noisy load pose estimate, while overestimating it may lead to an excessively free motion in the load estimate.

The EKF needs to be initialized with a first-order guess of load pose and twist, and cable directions. We assume a static initial load state, namely a zero twist. As for the load pose and cable directions, we propose an algorithm to provide a guess through Kabsch-Umeyama algorithm (38). The details of the algorithm are provided in Algorithm 1.

4.4 Trajectory tracking controller on quadrotors

Every 100 ms, the most recently generated reference trajectories by the planner are sent to each quadrotor, and processed by a differential-flatness-based trajectory tracking controller deployed onboard, modified from (27). Since the trajectory tracking controller operates at a higher frequency 300 Hz than the interval between nodes in the reference trajectory, a time-based sampler is implemented to generate high-frequency reference states by linearly interpolating between the discretized nodes of the reference trajectory. The sampler continues to sample along the reference trajectory until a new reference is received.

The onboard trajectory tracking controller computes the thrust command using position and velocity feedback, as well as feedforward terms that include the acceleration reference, and external

Algorithm 1 Iterative Kabsch-Umeyama algorithm to initialize states of the EKF

Define tolerance and maximum steps for iteration: $tol_{\text{pos}}, tol_{\text{att}}, iter_{\text{max}}$

Number of quadrotors n

Average cable connection points $\bar{\rho} = \sum_i^n \rho_i/n$, $L = [\rho_1 - \bar{\rho}, \rho_2 - \bar{\rho}, \dots, \rho_n - \bar{\rho}]$

Define initial load pose $\mathbf{p} = [0, 0, 0]^\top$, $\mathbf{R} = \mathbf{I}_3$

Initialize the last load pose $\mathbf{p}_{\text{last}} = \text{inf}$, $\mathbf{R}_{\text{last}} = \mathbf{O}_3$

Initial guess of cable directions

Initial guess of cable directions $\mathbf{s}_i = [0, 0, -1]^\top$ for $i = \{1, 2, \dots, n\}$

for $k = 1, \dots, iter_{\text{max}}$ **do**

for $i = 1, \dots, n$ **do**

$$\mathbf{c}_i = \mathbf{p}_i + \mathbf{s}_i l_i$$

$$\bar{\mathbf{c}} = \sum_{i=1}^n \mathbf{c}_i/n$$

$$\mathbf{C} = [\mathbf{c}_1 - \bar{\mathbf{c}}, \mathbf{c}_2 - \bar{\mathbf{c}}, \dots, \mathbf{c}_n - \bar{\mathbf{c}}]$$

$$[\mathbf{U}, \mathbf{V}] = \text{SVD}(\mathbf{L}\mathbf{C}^\top)$$

$$\mathbf{R} = \mathbf{V} \begin{bmatrix} 1 & 0 & 0 \\ 0 & 1 & 0 \\ 0 & 0 & \text{sign}(\det(\mathbf{V}\mathbf{U}^\top)) \end{bmatrix} \mathbf{U}^\top$$

▸ Estimated load attitude

for $i = 1, 2, \dots, n$ **do**

$$\tilde{\mathbf{p}}_i = \mathbf{c}_i - \mathbf{R}\rho_i$$

$$\mathbf{p} = \sum_{i=1}^n \tilde{\mathbf{p}}_i/n$$

▸ Estimated load position

for $i = 1, 2, \dots, n$ **do**

$$\mathbf{s}_i = (\mathbf{R}\rho_i + \mathbf{p} - \mathbf{p}_i) / \|\mathbf{R}\rho_i + \mathbf{p} - \mathbf{p}_i\|$$

▸ Estimated cable direction

if $\|\mathbf{p} - \mathbf{p}_{\text{last}}\| < tol_{\text{pos}}$ **and** $\det(\mathbf{R}^{-1}\mathbf{R}_{\text{last}}) < tol_{\text{att}}$ **then**

Break

$$\mathbf{p}_{\text{last}} = \mathbf{p}, \mathbf{R}_{\text{last}} = \mathbf{R}$$

Return $\mathbf{p}, \mathbf{q}(\mathbf{R}), \mathbf{s}_1, \mathbf{s}_2, \dots, \mathbf{s}_n$

forces due to the cable tension and aerodynamic drag

$$T_{i,\text{des}}z_{i,\text{des}}/m_i = \mathbf{K}_p (\mathbf{p}_{i,\text{ref}} - \mathbf{p}_i) + \mathbf{K}_v (\mathbf{v}_{i,\text{ref}} - \mathbf{v}_i) + \dot{\mathbf{v}}_{i,\text{ref}} + \mathbf{f}_{\text{ext}}/m_i \quad (15)$$

where $\mathbf{K}_p \in \mathbb{R}^{3 \times 3}$ and $\mathbf{K}_v \in \mathbb{R}^{3 \times 3}$ are positive definite gain matrices.

The cable and aerodynamic forces are estimated using the accelerometer on the quadrotor through the relationship $\mathbf{f}_{\text{ext}} = m_i \mathbf{a}_{i,\text{filtered}} - \mathbf{f}_{i,\text{filtered}}$, where $\mathbf{a}_{i,\text{filtered}}$ is the unbiased and low-pass-filtered accelerometer measurement, $\mathbf{f}_{i,\text{filtered}}$ is the current collective thrust denoised with the same filter. Then, we use a tilt-prioritized attitude controller (39) to generate the angular acceleration command from the desired attitude $z_{i,\text{des}}$, the reference jerk, and the zero yaw rate reference.

The angular acceleration and force commands are eventually allocated to rotor speed commands through an INDI inner-loop controller, which is robust against external torque disturbances such as aerodynamic torque, motor differences, quadrotor CoG bias, etc. We omit the details of INDI and refer interested readers to (25–27) for further information.

References

1. D. Hanover, P. Foehn, S. Sun, E. Kaufmann, D. Scaramuzza, Performance, precision, and payloads: Adaptive nonlinear mpc for quadrotors. *IEEE Robotics and Automation Letters* **7** (2), 690–697 (2021).
2. A. Saviolo, G. Loianno, Learning quadrotor dynamics for precise, safe, and agile flight control. *Annual Reviews in Control* **55**, 45–60 (2023).
3. G. Loianno, V. Kumar, Cooperative transportation using small quadrotors using monocular vision and inertial sensing. *IEEE Robotics and Automation Letters* **3** (2), 680–687 (2017).
4. A. Tagliabue, M. Kamel, S. Verling, R. Siegwart, J. Nieto, Collaborative transportation using mavs via passive force control, in *2017 IEEE International Conference on Robotics and Automation (ICRA)* (IEEE) (2017), pp. 5766–5773.
5. A. Tagliabue, M. Kamel, R. Siegwart, J. Nieto, Robust collaborative object transportation using multiple MAVs. *The International Journal of Robotics Research* **38** (9), 1020–1044 (2019).
6. J. Balaram, M. Aung, M. P. Golombek, The ingenuity helicopter on the perseverance rover. *Space Science Reviews* **217** (4), 56 (2021).
7. R. D. Lorenz, *et al.*, Dragonfly: A rotorcraft lander concept for scientific exploration at Titan. *Johns Hopkins APL Technical Digest* **34** (3), 14 (2018).
8. N. Michael, J. Fink, V. Kumar, Cooperative manipulation and transportation with aerial robots. *Autonomous Robots* **30**, 73–86 (2011).
9. K. Sreenath, V. Kumar, Dynamics, control and planning for cooperative manipulation of payloads suspended by cables from multiple quadrotor robots, in *Robotics: science and systems (RSS)* (2013), p. 8p.
10. G. Li, R. Ge, G. Loianno, Cooperative transportation of cable suspended payloads with mavs using monocular vision and inertial sensing. *IEEE Robotics and Automation Letters* **6** (3), 5316–5323 (2021).
11. G. Li, G. Loianno, Nonlinear model predictive control for cooperative transportation and manipulation of cable suspended payloads with multiple quadrotors, in *2023 IEEE/RSJ International Conference on Intelligent Robots and Systems (IROS)* (IEEE) (2023), pp. 5034–5041.
12. T. Lee, K. Sreenath, V. Kumar, Geometric control of cooperating multiple quadrotor UAVs with a suspended payload, in *52nd IEEE conference on decision and control* (IEEE) (2013), pp. 5510–5515.

13. T. Lee, Geometric control of quadrotor UAVs transporting a cable-suspended rigid body. *IEEE Transactions on Control Systems Technology* **26** (1), 255–264 (2017).
14. J. Geng, P. Singla, J. W. Langelaan, Load-distribution-based trajectory planning and control for a multilift system. *Journal of Aerospace Information Systems* **19** (5), 366–381 (2022).
15. K. Wahba, W. Hönig, Efficient optimization-based cable force allocation for geometric control of a multirotor team transporting a payload. *IEEE Robotics and Automation Letters* (2024).
16. K. Wahba, J. Ortiz-Haro, M. Toussaint, W. Hönig, Kinodynamic Motion Planning for a Team of Multirotors Transporting a Cable-Suspended Payload in Cluttered Environments. *arXiv preprint arXiv:2310.03394* (2023).
17. M. Manubens, D. Devaurs, L. Ros, J. Cortés, Motion planning for 6-D manipulation with aerial towed-cable systems, in *Robotics: science and systems (RSS)* (2013), p. 8p.
18. E. Fresk, G. Nikolakopoulos, Full quaternion based attitude control for a quadrotor, in *2013 European control conference (ECC)* (IEEE) (2013), pp. 3864–3869.
19. D. Sanalitra, H. J. Savino, M. Tognon, J. Cortés, A. Franchi, Full-pose manipulation control of a cable-suspended load with multiple UAVs under uncertainties. *IEEE Robotics and Automation Letters* **5** (2), 2185–2191 (2020).
20. C. Masone, P. Stegagno, Shared control of an aerial cooperative transportation system with a cable-suspended payload. *Journal of Intelligent & Robotic Systems* **103** (3), 40 (2021).
21. S. Sun, A. Franchi, Nonlinear MPC for full-pose manipulation of a cable-suspended load using multiple UAVs, in *2023 International Conference on Unmanned Aircraft Systems (ICUAS)* (IEEE) (2023), pp. 969–975.
22. G. Li, X. Liu, G. Loianno, RotorTM: A flexible simulator for aerial transportation and manipulation. *IEEE Transactions on Robotics* (2023).
23. M. Bernard, K. Kondak, G. Hommel, Load transportation system based on autonomous small size helicopters. *The aeronautical journal* **114** (1153), 191–198 (2010).
24. M. Bernard, K. Kondak, I. Maza, A. Ollero, Autonomous transportation and deployment with aerial robots for search and rescue missions. *Journal of Field Robotics* **28** (6), 914–931 (2011).
25. E. J. Smeur, Q. Chu, G. C. De Croon, Adaptive incremental nonlinear dynamic inversion for attitude control of micro air vehicles. *Journal of Guidance, Control, and Dynamics* **39** (3), 450–461 (2016).

26. E. Tal, S. Karaman, Accurate tracking of aggressive quadrotor trajectories using incremental nonlinear dynamic inversion and differential flatness. *IEEE Transactions on Control Systems Technology* **29** (3), 1203–1218 (2020).
27. S. Sun, A. Romero, P. Foehn, E. Kaufmann, D. Scaramuzza, A comparative study of nonlinear mpc and differential-flatness-based control for quadrotor agile flight. *IEEE Transactions on Robotics* **38** (6), 3357–3373 (2022).
28. D. Mellinger, V. Kumar, Minimum snap trajectory generation and control for quadrotors, in *2011 IEEE international conference on robotics and automation (IEEE)* (2011), pp. 2520–2525.
29. P. Foehn, *et al.*, Agilicious: Open-source and open-hardware agile quadrotor for vision-based flight. *Science robotics* **7** (67), eabl6259 (2022).
30. A. Petitti, *et al.*, Inertial estimation and energy-efficient control of a cable-suspended load with a team of UAVs, in *2020 International Conference on Unmanned Aircraft Systems (ICUAS)* (IEEE) (2020), pp. 158–165.
31. A. Richards, J. How, Robust stable model predictive control with constraint tightening, in *2006 American Control Conference (IEEE)* (2006), pp. 6–pp.
32. J. Köhler, M. A. Müller, F. Allgöwer, A novel constraint tightening approach for nonlinear robust model predictive control, in *2018 Annual American control conference (ACC)* (IEEE) (2018), pp. 728–734.
33. P. Foehn, A. Romero, D. Scaramuzza, Time-optimal planning for quadrotor waypoint flight. *Science robotics* **6** (56), eabh1221 (2021).
34. H. G. Bock, K.-J. Plitt, A multiple shooting algorithm for direct solution of optimal control problems. *IFAC Proceedings Volumes* **17** (2), 1603–1608 (1984).
35. M. Diehl, *et al.*, Real-time optimization and nonlinear model predictive control of processes governed by differential-algebraic equations. *Journal of Process Control* **12** (4), 577–585 (2002).
36. R. Verschueren, *et al.*, acados—a modular open-source framework for fast embedded optimal control. *Mathematical Programming Computation* **14** (1), 147–183 (2022).
37. M. Faessler, A. Franchi, D. Scaramuzza, Differential flatness of quadrotor dynamics subject to rotor drag for accurate tracking of high-speed trajectories. *IEEE Robotics and Automation Letters* **3** (2), 620–626 (2017).

38. S. Umeyama, Least-squares estimation of transformation parameters between two point patterns. *IEEE Transactions on Pattern Analysis & Machine Intelligence* **13** (04), 376–380 (1991).
39. D. Brescianini, R. D’Andrea, Tilt-prioritized quadrocopter attitude control. *IEEE Transactions on Control Systems Technology* **28** (2), 376–387 (2018).

Appendix

Proof of Smoothness of Quadrotor Trajectories

Proposition 1 *When the i -th cable remains taut, the trajectory of i -th quadrotor, denoted as $\mathbf{p}_i(t)$, is C^3 smooth if λ_i and γ_i defined in equation 3 are bounded.*

Proof: For the i -th quadrotor, the kinematic constraint (Equation 5) holds when the corresponding cable is taut. Then we take the 3rd-order derivative of Equation 5 to obtain the jerk of the quadrotor

$$\begin{aligned} \ddot{\mathbf{v}}_i = & \ddot{\mathbf{v}} + \mathbf{R}(\mathbf{q}) \left\{ \boldsymbol{\omega} \times \left[\dot{\boldsymbol{\omega}} \times \boldsymbol{\rho}_i + \boldsymbol{\omega} \times (\boldsymbol{\omega} \times \boldsymbol{\rho}_i) \right] \right. \\ & \left. + \ddot{\boldsymbol{\omega}} \times \boldsymbol{\rho}_i + \dot{\boldsymbol{\omega}} \times (\boldsymbol{\omega} \times \boldsymbol{\rho}_i) + \boldsymbol{\omega} \times (\dot{\boldsymbol{\omega}} \times \boldsymbol{\rho}_i) \right\} \\ & - l_i \left\{ \ddot{\mathbf{r}}_i \times \mathbf{s}_i + 2\dot{\mathbf{r}}_i \times (\mathbf{r}_i \times \mathbf{s}_i) + \mathbf{r}_i \times (\dot{\mathbf{r}}_i \times \mathbf{s}_i) \right. \\ & \left. + \mathbf{r}_i \times \left[\mathbf{r}_i \times (\mathbf{r}_i \times \mathbf{s}_i) \right] \right\} \end{aligned} \quad (16)$$

where $\dot{\mathbf{v}}$ and $\dot{\boldsymbol{\omega}}$ are given in the load dynamics (Equation 2), $\ddot{\mathbf{v}}$ and $\ddot{\boldsymbol{\omega}}$ are obtained by taking the derivative of both sides of Equation 2

$$\ddot{\mathbf{v}} = -\frac{1}{m} \sum_{i=1}^n \left[\dot{t}_i \mathbf{s}_i + t_i (\mathbf{r}_i \times \mathbf{s}_i) \right] \quad (17)$$

$$\ddot{\boldsymbol{\omega}} = \mathbf{J}^{-1} \left\{ -\dot{\boldsymbol{\omega}} \times \mathbf{J}\boldsymbol{\omega} - \boldsymbol{\omega} \times \mathbf{J}\dot{\boldsymbol{\omega}} + \sum_{i=1}^n \left[\dot{t}_i \mathbf{R}^\top \mathbf{s}_i + t_i \left(-\boldsymbol{\omega} \times \mathbf{R}^\top \mathbf{s}_i + \mathbf{R}^\top (\mathbf{r}_i \times \mathbf{s}_i) \right) \right] \times \boldsymbol{\rho}_i \right\} \quad (18)$$

Judging from the load-cable dynamics (Equation 2 and 3), the continuousness of $\ddot{\mathbf{v}}_i$ is determined by the highest-order states \dot{t}_i and $\dot{\mathbf{r}}_i$. Therefore, $\ddot{\mathbf{v}}_i$ is continuous, namely the \mathbf{p}_i is C^3 -smooth, when $\dot{t}_i = \gamma_i$ and $\dot{\mathbf{r}}_i = \lambda_i$ are bounded.

The OCP of the planner takes γ_i and λ_i as inputs, which can be bounded by setting input constraints. Hence the generated trajectories of all quadrotors are smooth up jerk as long as the cable tautness is guaranteed. One step further, once the reference jerk is continuous, we can also obtain a smooth angular velocity reference.

Proposition 2 *The angular velocity of the i -th quadrotor expressed in the inertial frame, denoted by $\boldsymbol{\omega}_i^{\mathcal{I}} \in \mathbb{R}^3$ is C^0 -smooth if λ_i and γ_i defined in Equation 3 are bounded, and aerodynamic drag $\mathbf{f}_{a,i}$ is at least C^1 -smooth.*

Proof: To obtain the angular velocity reference of each quadrotor, we need to revisit the translational dynamic equation of the i -th quadrotor

$$\dot{\mathbf{v}}_i = (T_i \mathbf{z}_i + t_i \mathbf{s}_i + \mathbf{f}_{a,i}) / m_i + \mathbf{g} \quad (19)$$

Taking derivative of both side of Equation 19, we have

$$\begin{aligned} \mathbf{h}_i &\triangleq \boldsymbol{\omega}_i^{\mathcal{I}} \times \mathbf{z}_i \\ &= \left[m_i \ddot{\mathbf{v}}_i - \dot{T}_i \mathbf{z}_i - \dot{t}_i \mathbf{s}_i - t_i (\mathbf{r}_i \times \mathbf{s}_i) - \dot{\mathbf{f}}_{a,i} \right] / T_i \end{aligned} \quad (20)$$

Since the yaw rate references are zero for all quadrotors, $\boldsymbol{\omega}_i^{\mathcal{I}}$ is perpendicular to \mathbf{z}_i . Then we can obtain the expression of $\boldsymbol{\omega}_i^{\mathcal{I}}$ by

$$\boldsymbol{\omega}_i^{\mathcal{I}} = \mathbf{z}_i \times \mathbf{h}_i = \frac{1}{T_i} \mathbf{z}_i \times \left[\ddot{\mathbf{v}}_i - \dot{t}_i \mathbf{s}_i - t_i (\mathbf{r}_i \times \mathbf{s}_i) - \dot{\mathbf{f}}_{a,i} \right] \quad (21)$$

According to Proposition 1 and Equation 9, $\ddot{\mathbf{v}}_i$ is C^0 -smooth and T_i is at least C^1 smooth. When γ_i is bounded, \dot{t}_i is also C^0 -smooth. Hence angular velocity $\boldsymbol{\omega}_i^{\mathcal{I}}$ is also C^0 -smooth when $\mathbf{f}_{a,i}$ is at least C^1 -smooth. If we use Equation 21 to generate the angular velocity reference of each quadrotor, its smoothness is guaranteed through Proposition 2, if we use a smooth drag model (In this work, we assume a zero drag for simplicity). The smooth angular velocity reference, used as feed-forward terms by the trajectory tracking controller onboard the quadrotor, guarantees smooth quadrotor behavior, which is particularly crucial during dynamic motions.